A peer-reviewed version of this preprint was published in PeerJ on 5 February 2015.

Arnhold F, Gührs K, von Mikecz A. 2015. Amyloid domains in the cell nucleus controlled by nucleoskeletal protein lamin B1 reveal a new pathway of mercury neurotoxicity. PeerJ 3:e754
https://doi.org/10.7717/peerj.754

Amyloid domains in the cell nucleus controlled by nucleoskeletal protein lamin B1 reveal a new pathway of mercury neurotoxicity

Florian Arnhold, Karl-Heinz Guehrs, Anna von Mikecz

Mercury (Hg) is a bioaccumulating trace metal that globally circulates the atmosphere and waters in its elemental, inorganic and organic chemical forms. While Hg represents a notorious neurotoxicant, the underlying cellular pathways are insufficiently understood. We identify amyloid protein aggregation in the cell nucleus as a novel pathway of Hg-bio-interactions. By mass spectrometry of purified protein aggregates a subset of spliceosomal components and nucleoskeletal protein lamin B1 were detected as constituent parts of an Hg-induced nuclear aggregome network. The aggregome network was located by confocal imaging of amyloid-specific antibodies and dyes to amyloid cores within splicing-speckles that additionally recruit components of the ubiquitin-proteasome system. Hg significantly enhances global proteasomal activity in the nucleus suggesting that formation of amyloid speckles plays a role in maintenance of protein homeostasis. RNAi knock down showed that lamin B1 for its part regulates amyloid speckle formation and thus likewise participates in nuclear protein homeostasis. As the Hg-induced cascade of interactions between the nucleoskeleton and protein homeostasis reduces neuronal signalling, amyloid fibrillation in the cell nucleus is introduced as a feature of Hg-neurotoxicity that opens new avenues of future research. Similar to protein aggregation events in the cytoplasm that are controlled by the cytoskeleton, amyloid fibrillation of nuclear proteins may be driven by the nucleoskeleton.

Amyloid domains in the cell nucleus controlled by nucleoskeletal protein lamin B1 reveal a new pathway of mercury neurotoxicity

Florian Arnhold[1], Karl-Heinz Gührs[2] and Anna von Mikecz[1,*]

[1]IUF - Leibniz Research Institute for Environmental Medicine at Heinrich-Heine-University Duesseldorf, Duesseldorf, Germany

[2]CF Proteomics, FLI - Leibniz-Institute for Age Research, Fritz-Lipman-Institute e.V., Jena, Germany

[*]Corresponding author:

Anna von Mikecz, Dr. rer. nat.

Professor of Genetics

IUF - Leibniz Research Institute for Environmental Medicine at Heinrich-Heine-University Duesseldorf

Auf'm Hennekamp 50

40225 Duesseldorf

Germany

fon: ++49-211-3389-358

email: mikecz@tec-source.de

Key words: Amyloid, lamin B, mercury, ribonucleoproteins, protein fibrillation, proteomics, RNA splicing

30 Short title: Lamin B1 controlled nuclear amyloid

INTRODUCTION

The heavy metal mercury (Hg) represents a global pollutant that is released predominantly due to anthropogenic activities including artisanal gold mining, metal or cement production, coal-burning and fossil fuel combustion [Streets et al., 2011; UNEP, 2013; Amos et al., 2014]. Global circulation of Hg is now inventoried throughout the Pacific and Atlantic oceans [Lamborg, 2014] and best reflected by its detection in marine food chains of remote areas such as the Arctic [Bocharova, 2013]. Seafood-rich diets result in elevated total Hg concentrations of hair, cord blood or human transition milk samples and have been correlated with mild cognitive deficits in cohorts of prenatally exposed school children [Grandjean, 1995, 1997]. While Hg represents an acknowledged neurotoxicant, little is known about the molecular pathways leading to adverse biological end points such as impairment of neural functions and neurodegeneration [Eto, 1997; Axelrad et al., 2007; Korbas et al., 2010]. This is particularly noteworthy since inorganic mercury (I-Hg) that currently provides the best available marker for assessment of chronic exposures rises in the US population [Laks, 2014].

A prominent molecular pathway of neurodegeneration is amyloid protein fibrillation that occurs (i) spontaneously in systemic amyloidoses and neurodegenerative aggregation diseases [Goedert, 2001; Ross and Poirier, 2004] or (ii) after experimental induction *in vitro*, for example by exposition of biochemically purified proteins or mammalian cell culture to heavy metals [Uversky et al., 2001; Chen et al., 2008]. Protein aggregates in nuclei of brain cells are a hallmark of a number of neurodegenerative triplet repeat diseases such as Huntington's disease (HD). In the HD cortex and striatum intranuclear protein aggregates contain mutant huntingtin that has a CAG (polyglutamine, polyQ) repeat expansion as well as additional proteins such as ubiquitin suggesting involvement of proteasomal proteolysis in the formation of amyloid inclusions [DiFiglia et al., 1997]. Nuclear co-aggregation of huntingtin, ubiquitin and proteasomes was likewise observed in brains from mice transgenic for the HD mutation [Davies et al., 1997]. Notably, nuclei of HD mice display a distinct

morphology, since their nuclear envelope changes to an irregular shape [Davies et al., 1997]. In addition to components of the ubiquitin-proteasome system other nuclear proteins such as transcriptional co-activator CREB-binding protein (CBP) and the general transcription factor TATA-binding protein (TBP) were shown to co-aggregate in nuclear protein inclusions of patients with triplet repeat diseases suggesting that a variety of aggregation-prone proteins contribute to amyloid-like protein fibrillation in the nucleus [Perez et al., 1998; von Mikecz, 2014].

Intracellular congestion of otherwise soluble proteins to amyloid-like, sodium dodecyl sulfate (SDS)-resistant protein aggregates proceeds in sequential steps. The current conception delineates the transition of globular proteins through conformational changes of native monomers via oligomeric intermediates to highly ordered amyloid fibrils that may be initiated by locally unfolded states of the native protein [Chiti and Dobson, 2009; Knowles, 2014; Uversky, 2014]. Amyloid-like intermediates as well as amyloid fibers are detectable by solid-state nuclear magnetic resonance, electron microscopy and a variety of dyes including Congo red (CR) or Thioflavin T (ThT). Intracellular amyloid can be localized by means of amyloid-specific antibodies [O'Nuallain and Wetzel, 2002] or peptides [Wiesehahn et al., 2003] and the before mentioned amyloid-binding dyes. Systems that mimic the process of nuclear protein aggregation / fibrillation *in vitro* by protein over-expression suggest a mechanism of conjoint sequestration of expanded polyQ proteins, unexpanded polyQ proteins and aggregation-prone nuclear proteins [von Mikecz, 2014].

In this study we identify protein fibrillation to nuclear amyloid as a pathway that is induced by environmentally relevant concentrations of I-Hg. In an unbiased proteomic approach nuclear amyloid was isolated biochemically and its proteinaceous composition characterized by subsequent mass spectrometry (MS) showing that components of the splicing machinery constitute a major component of an I-Hg-induced nuclear aggregome. In line with this, confocal imaging demonstrates that the core of nuclear speckles enriched with spliceosomal components, undergoes stepwise protein fibrillation to

amyloid microenvironments. I-Hg-induced nuclear amyloid is correlated with altered RNA processing, specific activation of the nuclear ubiquitin-proteasome system and exclusively forms under the control of nucleoskeletal protein lamin B1 that MS analysis likewise identified as a component of the nuclear aggregome. Such interactions between the nucleoskeleton and nuclear protein homeostasis represent a novel molecular pathway of Hg-(neuro)toxicity that reduces neural signalling and clearly resembles the nuclear pathology observed in neurodegenerative aggregation diseases.

MATERIALS AND METHODS

Cell culture

SH-SY5Y cells (American Tissue Culture Collection) were cultured in a humidified atmosphere with 5% CO_2 at 37°C. D-MEM/F-12 (1:1) medium, supplemented with 15% FCS and 1% penicillin/ streptomycin, was used as growth/ proliferation medium. To induce neuronal differentiation SH-SY5Y cells were cultured in serum-free Neurobasal™ medium with neural cell supplement (B-27), 10µM retinoic acid, 1% L-glutamine and 1% penicillin/ streptomycin (Gibco, Life Technologies) for seven days. All experiments were performed with differentiated, post-mitotic SH-SY5Y cells. HEp-2 cells (American Tissue Culture Collection) were cultured under the same atmospheric conditions in RPMI1640 medium supplemented with 10% fetal calf serum (FCS) and 5% supplement complete (SC). Cells were treated for four hours or as indicated with 25 µM (SH-SY5Y) or 60 µM (HEp-2) I-Hg, *e.g.* mercuric chloride ($HgCl_2$, Merck KGaA). These treatment protocols were established according to results from atomic absorption spectroscopy of nuclear cell fractions (Table 1) and titration of I-Hg concentrations that do not induce cell death (Supplemental Fig. S1).

Cell viability assay

Cells were seeded simultaneously in culture flasks with the same density and left untreated or treated with I-Hg. At the indicated times, cells were trypsinized and counted by hemocytometer (n = 100 – 200). Cell viability was assessed by Trypan blue exclusion.

Atomic Absorption Spectroscopy (AAS)

HEp-2 cells were cultured as indicated and fractionated according to subcellular compartments as reported previously [Rockel et al., 2005]. Immunoblot detection of calnexin or SmB/B' was used to control for purity of cytoplasmic or nuclear fractions, respectively. Equal loading was controlled by Coomassie Brilliant Blue staining. $6*10^6$ cells were used in each fraction. Hg concentrations of the cell fractions were determined by cold vapor atomic absorption spectroscopy as described previously [Wilhelm et al., 2003]. To calculate the wet weight and the dry weight of the samples, cellular fractions were prepared as described above. The nuclear pellet, *e.g.* the nuclear fraction resulting from centrifugation and separation of the cytoplasmic supernatant, was defined as wet weight. For determinations of the dry weight cellular fractions in lysis buffer were heat- and air dried (80°C) for 6 hours.

Antibodies

The following antibodies were used for immunofluorescence, filter retardation and/ or western blot: WO1 amyloid-specific antibody (mouse monoclonal) [O'Nuallain and Wetzel, 2002], beta tubulin (mouse monoclonal, TUB 2.1, Sigma-Aldrich), FUS/TLS (rabbit monoclonal, EPR5812, Abcam), hsc70 (rabbit monoclonal, EP1531Y, Abcam), lamin B (goat polyclonal, C-20, Santa Cruz Biotechnology, Inc.), lamin A/C (mouse monoclonal, Santa Cruz Biotechnology Inc.), nucleolin C23 (mouse monoclonal, MS-3, Santa Cruz Biotechnology Inc.), nucleophosmin B23 (rabbit polyclonal, H-106, Santa Cruz Biotechnology Inc.), U1-70K/SmB/B' (human serum, ASR53, von Mikecz serum database), ubiquitin (rabbit polyclonal, Sigma-Aldrich), polyQ (mouse monoclonal, 5TF1-1C2 MAB1574, Millipore), pan hnRNP (mouse monoclonal, C-6, Santa Cruz Biotechnology Inc.), calnexin (rabbit polyclonal, Santa Cruz Biotechnology Inc.), 20S proteasome alpha subunits (mouse monoclonal, MCP231, Millipore), 20S proteasome (rabbit polyclonal, kind gift of B. Dahlmann), CaMKII alpha (mouse monoclonal, Abcam), CaMKII alpha phospho T286 (rabbit polyclonal, Abcam).

Imaging

For confocal immunofluorescence (IF) microscopy cells were grown on cover slips to subconfluence, fixed with methanol (-20°C, 5 minutes) and permeabilized with ice-cold acetone (-20°C, 2 minutes). After washing with PBS the cells were incubated with the primary antibody for 1 hour and washed with PBS. The secondary antibody (conjugated with FITC, Rhodamin or Cy5) was incubated for 45 minutes. Cells were washed with PBS, covered in mounting medium (Vectashield, Vector Labs) and stored at 4°C in the dark. To detect intracellular amyloid methanol/ acetone-fixed cells were incubated with amyloid dyes Congo red (Sigma-Aldrich) or Thioflavin T (Sigma-Aldrich) for 10 minutes. After washing with PBS, cells were covered in mounting medium and stored at 4°C in the dark. Immunostained or dye-stained cells were imaged using a confocal laser scanning microscope (Fluoview, IX70, Olympus) with a 60x/1.4NA Plan Apo objective. Congo red labelling was recorded with 568 nm excitation and micrographs of single nuclei are presented as pseudocolor intensity map using Metamorph 4.6 software.

Ca^{2+}-imaging

SH-SY5Y cells were differentiated with retinoic acid (RA; Sigma-Aldrich) for five days and for additional seven days with brain-derived neurotrophic factor (BDNF; Sigma-Aldrich). Intracellular Ca^{2+}-levels of living cells were visualized by the Fluo-4 Direct™ Calcium Assay Kit (Molecular Probes, Invitrogen) according to the manufacturer's instructions. Cells were imaged by confocal laser scanning microscopy (Fluoview, IX70, Olympus; 60x/1.4NA Plan Apo objective; low resolution/ high speed settings) with 0.5 Hz. Intracellular Fluo-4 intensity was quantified with Metamorph 4.6 software by intensity measurements within regions of interest (ROIs) for each cell and time point. The stimulation

response of each cell was calculated by the difference [%] between base line intensity and maximum peak intensity.

SDS-PAGE

Cells were cultured, harvested and lysed in loading buffer (0.05 M Trizma-HCl, pH 6.8, 0.1 M DTT, 2% SDS, 0.1% bromophenol blue, 10% glycerin) or fractionated into cytoplasmic and nuclear proteins as reported previously [Rockel et al., 2005]. Equal numbers of untreated or treated (as indicated) cells were loaded. Proteins were separated by SDS-PAGE (BioRad) and transferred onto nitrocellulose membranes. SDS-PAGE gels were stained with Coomassie brilliant blue overnight and de-stained for 2.5 hours. Nitrocellulose membranes were stained with Ponceau S and used for subsequent immunodetection.

Filter retardation assay

A dot-blot filter retardation assay was applied to isolate SDS-resistant protein aggregates as previously described [Wanker et al., 1999]. In brief, cells were washed and harvested in PBS, spun down, and lysed on ice for 30 minutes in lysis buffer containing 50 mM Tris–HCl, pH 8.8, 100 mM NaCl, 5 mM $MgCl_2$, 0.5% Triton X-100, and 1 mM EDTA supplemented with a protease inhibitor cocktail (Sigma-Aldrich). Insoluble material was collected by centrifugation for 5 minutes at 14,000 rpm in a microfuge (Eppendorf) at 4°C. Pellets were resolved in DNase buffer containing 20 mM Tris–HCl, pH 8.0, 15 mM $MgCl_2$, and 0.5 mg/ml DNase I and incubated for 1 hour at 37°C. Incubation was terminated by adjusting the mixture to 20 mM EDTA, 2% SDS, and 50 mM DTT, followed by heating to 98°C for 5 minutes. Protein samples were further diluted in 2% SDS and filtered through a cellulose

acetate membrane (pore size 0.2 mm, Whatman) by applying a vacuum on a BIO-DOT device (BioRad), followed by two washing steps with 0.1% SDS.

Immunodetection

Cellulose acetate filters with trapped SDS-resistant protein aggregates or SDS-PAGE nitrocellulose membranes were blocked in PBS containing 0.5% Tween20 with 5% nonfat dried milk, followed by Western blot detection. Filters were incubated with primary antibodies for one hour, washed with PBS (containing 0.5% Tween20) and incubated with secondary antibodies (conjugated with peroxidase, Dianova) for 45 minutes. After washing with PBS (containing 0.5% Tween20) detection was performed with Amersham ECL detection reagent according to the manufacturer's instructions.

Mass spectrometry - sample preparation

Filter-trapped protein aggregates were eluted from the cellulose acetate membrane and resuspended by overnight incubation in 6 M guanidinium hydrochloride (GuaHCl). 10 µl 100 mM DTT was added to the GuaHCl solution and incubated for one hour at room temperature, followed by addition of 10 µl 500 mM iodoacetamide and an incubation for one hour. Next, samples were dialyzed (Xpress Micro Dialyzer, Scienova) against 25 mM ammonium bicarbonate (AmBic) for at least one hour, followed by a two hour dialysis against digest buffer (8% acetonitrile/ 25 mM AmBic). The sample solutions were transferred to 0.5 ml Eppendorf tubes and digested with 15 ng trypsin overnight. The samples were dried in a rotary evaporator, dissolved in 20 µl 0.1% formic acid (FA) in 5% acetonitrile, centrifuged for 2 minutes (14,000 rpm) and the supernatants were transferred to a

polypropylene-sample vial. 5 µl of each sample were further analyzed (where necessary, 15 µl were used for one measurement).

Mass spectrometry – measurement (ESI-LC/MS)

For mass spectrometry (MS) analysis the LTQ Orbitrap XL ETD (ThermoScientific) coupled to a nano-HPLC NanoLC 2D System AS 1 (Eksigent) was used. The samples were loaded onto a trap column (Robust Reversed Phase Solid Phase Extraction Trap 100 µm x 40 mm, NanoSeparations) and washed with 30 µl buffer A (5% acetonitrile/ 0.1% formic acid). The bound analytes were transferred to a separation column (75 µm x 100 mm, NanoSeparations) by applying a linear gradient from 0 to 38% of buffer B (80% acetonitrile/ 0.1% formic acid) over 76 minutes. The measured spectra were processed by ProteomeDiscoverer 1.3 (ThermoScientific) and searched against the SwissProt database by Mascot (MatrixScience) with the following search parameters: enzyme: trypsin with two allowed miss cleavages; fixed modification: carbamidomethylation of cysteine; variable modification: oxidation of methionine, phosphorylation of serine and threonine; measurement precision of precursor ions: 10 ppm; measurement precision of fragment ions: 0.8 Da. Data compilation was performed by ProteomeDiscoverer 1.3 (ThermoScientific) and Scaffold 3 (Proteome Software).

Aggregome database analysis – subcellular location

The subcellular location of the SDS-insoluble aggregate components identified by MS was defined according to the UniProtKB database. The annotation nucleus was designated as 'nucleus', annotation cytoplasm and annotations as cytoplasmic organelles (*i.e.* mitochondria) were designated as 'cytoplasm'. Proteins with database annotations for both, nucleus and cytoplasm, were subsumed

in the category 'nucleus & cytoplasm'. For analysis of the human proteome the complete UniProtKB database was used.

Aggregome database analysis – protein classification

The PANTHER (Protein ANalysis THrough Evolutionary Relationships) database v8.0 [Mi et al., 2013] was used to identify the cellular and molecular functions of the SDS-insoluble aggregate components. The annotation PANTHER protein class was used as a basic classification, and if necessary, revised by a manual modification of class names and protein class affiliation, based on literature and UniProtKB references.

Aggregome database analysis – quantification of protein features

Protein sequence and structure features were extracted from the UniProtKB database. The number of proteins with a feature [%] and the average number/ frequency of the feature within proteins were calculated and are presented as fold change of the corresponding values based on the complete human proteome. All calculations were done in Microsoft Excel. Database raw data was imported from the database *.tab file. The corresponding value of each protein feature was identified and listed for each protein. The lists were used to identify the occurrence of a feature in a certain protein and, in a second step, motifs of a respective feature, *i.e.* the number of features within proteins were quantified. Based on these values, mean values of the different groups (ground state HEp-2, I-Hg-induced HEp-2, ground state SH-SY5Y, I-Hg-induced SH-SY5Y and complete database) are calculated.

265 Aggregome database analysis – quantification of protein-protein interaction partners

266 The number of known interaction partners of each protein was extracted from the HIPPIE
267 (Human Integrated Protein-Protein Interaction rEference) database v1.5 [Schaefer et al., 2012]. The
268 database was imported to Microsoft Excel and the overall numbers of known interactions of each
269 protein were calculated. The Mann-Whitney test was used to test for significant differences between
270 the groups using OriginPro 8.6 (Originlab).

271

272 Aggregome database analysis – quantification of splicing components / complexes

273 SDS-insoluble aggregome components identified by MS analysis were further characterized in
274 a database search of spliceosomal components [Cvitkovic and Jurica, 2013]. Proteins were listed
275 according to spliceosomal component families and participation in different spliceosomal complexes/
276 subunits.

277

278 Proteasome activity assays

279 Proteasomal acitivity in cell fractions was determined by cleavage of the fluorogenic precursor
280 substrate N-Succinyl-Leu-Leu-Val-Tyr-7-amino-4-methylcoumarin (Suc-LLVY-AMC; Affiniti, Exeter,
281 UK). 10μM substrate was added to cellular fractions (~1x10^6 cells), and incubated in a reaction buffer
282 (500 mM Hepes, 10 mM EDTA, pH 7.6). Fluorescent increase resulting from degradation of Suc-
283 LLVY-AMC at 37°C was monitored over time by means of a fluorometer (Fluoroscan Ascent, Thermo
284 Labsystems, Santa Fe, NM) at 340 nm excitation and at 460 nm emission, using free AMC as a
285 standard. Resulting product curves were followed for up to 16 hours. Each value of fluorescence
286 intensity represents a mean value obtained from three independent experiments. After 2 hours of

activity measurement, 10μM proteasome inhibitor lactacystin (Alexis Biochemicals, San Diego, CA) was applied to the substrate / lysate reaction where indicated.

RNA interference

Cells were cultured at low density in 6-well plates or on coverslips and transfected with lamin B1 siRNA (30 pmol or 60 pmol, Santa Cruz Biotechnology Inc.) or a control siRNA with scrambled sequence (siRNA scr., 60 pmol, Santa Cruz) according to the manufacturer's instructions. 24 hours after transfection siRNA-treated cells were processed for immunoblotting or imaging. Each experiment was performed at least three times.

Worm cultivation

C. elegans wild-type strain N2 was obtained from the Caenorhabditis Genetics Center (CGC, University of Minnesota, USA). Worms were cultured at 20°C as described before [Brenner, 1974]. For I-Hg treatment, synchronized worms at late L4 stage were transferred to liquid S medium containing H_2O as negative control or 60 μM I-Hg. Worms were left untreated or exposed to I-Hg for 24 hours, fixed and stained with Congo red (0.7 mg/ml). Fixation, Congo red staining and imaging was performed as described before [Scharf et al., 2013].

RESULTS AND DISCUSSION

Environmentally relevant I-Hg concentrations in the nucleus reduces Ca^{2+}-signalling in neural cells

I-Hg was applied in all experiments as it currently represents the best available marker for chronic Hg-exposure and accumulates within the human body [Laks, 2014]. Furthermore methyl-(Me-)Hg was shown to be de-methylated and persistently deposited in brains of macaques as I-Hg (Table 1) [Vahter et al., 1995]. In order to apply environmentally relevant expositions of human cells, differentiated neural SH-SY5Y cells or proliferating HEp-2 cells were titrated with increasing concentrations of I-Hg and the cell viability was analyzed (Supplemental Fig. S1). Concentrations that did not induce cell death, *e.g.* 25 μM I-Hg in SH-SY5Y or 60 μM I-Hg in HEp-2 cells, were designated as "mild" and used in subsequent experiments. By atomic absorption spectroscopy (AAS) total Hg was determined in cell fractions that were left untreated or exposed to the higher I-Hg concentration of 60 μM (Supplemental Fig. S2) and compared with a variety of hair and organ samples from Hg-exposed animals or humans (Table 1). Due to the similar range of total Hg concentrations in nuclear fractions of I-Hg-treated HEp-2 cells, namely 2.74 ± 1.03 μg/g Hg wet weight and 6.08 ± 2.29 μg/g Hg dry weight, as compared with samples from humans and animals that fed on marine diets or experimentally exposed monkeys we consider the I-Hg concentrations applied in this study environmentally relevant.

Usage of differentiated SH-SY5Y cells offers the possibility to investigate effects of mild I-Hg concentrations on the neural system, as the brain represents both (i) one of the main deposition sites of I-Hg and Me-Hg and (ii) a respective target of neurotoxicity in exposed humans and animals (Table 1; [Clarkson and Magos, 2006]). As changes of intracellular Ca^{2+} levels represent an initial event of the neuronal signalling cascade we next analyzed Ca^{2+}-signalling in differentiated SH-SY5Y cells to determine if environmentally relevant concentrations of I-Hg effect neural activity. Ca^{2+}-influx was observed after stimulation of SH-SY5Y neurons with KCl or the cholinergic agonist carbachol by measuring the fluorescence intensity of the Ca^{2+}-indicator Fluo 4 over time. The addition of both, KCl as well as carbachol concurred with an immediate peak of Fluo 4 intensity that linearly regressed to the basal level within the next 20 seconds of the measurements (Fig. 1, A and C). A difference

between untreated (Fig. 1, A and C; solid line) and I-Hg-treated (dotted line) SH-SY5Y cells was identified as I-Hg-exposure reduced the peak intensity under conditions of KCl or carbachol stimulation significantly (Fig. 1, B and D). Notably, I-Hg reduces the carbachol stimulated Ca^{2+}-influx to a higher extent than the response to stimulation by KCl suggesting that neuro-specific signalling is more susceptible.

To characterize the downstream signalling cascade of neural processing we analyzed the activation of the protein Ca^{2+} / calmodulin-dependent protein kinase II (CaMKII) (Fig. 1, E and F). CaMKII regulates long-term potentiation and is activated by phosphorylation of the tyrosine residue at position 286 (T286) [Malinow et al., 1988]. Immunoblotting shows that after stimulation of untreated SH-SY5Y neurons with KCl or carbachol expression of T286-phospho CaMKII is significantly induced by about 5-fold (Fig. 1E, lanes 1-3). In contrast, a significantly reduced activation of CaMKII phosphorylation was observed in I-Hg-treated SH-SY5Y neurons (Fig. 1E, lanes 4-6). Consistent with the results from intracellular Ca^{2+}-imaging carbachol stimulation is more susceptible to I-Hg-exposure, since expression of T286-phospho CaMKII is not significantly induced in comparison with unstimulated neurons, *e.g.* I-Hg impairs activation of CaMKII by phosphorylation (Fig. 1E, lanes 4 and 6). Stimulation-specific activation of phosphorylated CaMKII was corroborated by comparison with total CaMKII that showed equal expression in all conditions of I-Hg-treatment with or without modulation of Ca^{2+}-influx by KCl or carbachol (Fig. 1E, lanes 1-6). Taken together we show that environmentally relevant concentrations of I-Hg interfere with initial and downstream steps of the Ca^{2+}-signalling cascade thereby exerting adverse effects on neural function by reduction of the excitation plasticity. Further studies are needed to investigate in detail the nature of the interactions between I-Hg accumulation in the cell nucleus (Table 1) and failure of neuronal signaling, *e.g.* supposable direct interactions of I-Hg with neuronal receptors and synaptic function.

Amyloid microenvironments are induced by environmentally relevant concentrations of I-Hg

Due to previous reports that metals induce protein fibrillation *in* vitro [Uversky et al., 2001], local amyloid was imaged after I-Hg exposition in human epithelial HEp-2 and neural SH-SY5Y cells by confocal microscopy using different detection reagents. The monoclonal antibody WO1 recognizes conformational epitopes of all amyloid fibrils and amyloid-like aggregates [O'Nuallain and Wetzel, 2002]. In the nucleus WO1 labels nucleoli and speckled domains in the nucleoplasm (Fig. 2, A and B). The staining pattern is of low intensity in untreated or ground state HEp-2 cells (Fig. 2A), but distinct and of high intensity in cells exposed to I-Hg (Fig. 2B). Notably, environmentally relevant concentrations of I-Hg induce the aggregation of soluble proteins or oligomers in amyloid-like nuclear microenvironments, while cell viability remains unchanged (Supplemental Fig. S1). In agreement with these results staining of I-Hg-treated cells with amyloid-binding dyes Thioflavin T (ThT) and Congo red (CR) showed intensified labelling of nucleoli and the nucleoplasm (Fig. 2, D and F). In contrast to immunolabelling with WO1, the dyes ThT and CR undergo a pattern change in the nucleoplasm from a diffuse homogeneous to an intensified, speckled staining pattern that might indicate the transition of the protein fibrillation state from oligomeric intermediates throughout the nucleoplasm to formation of amyloid-like protein aggregates in distinct nuclear microdomains. Consistent with this idea WO1 that detects highly ordered amyloid fibrils but not oligomeric intermediates [O'Nuallain and Wetzel, 2002], exclusively labels amyloid microenvironments with a speckled phenotype in the nucleoplasm (Fig. 2B; arrowhead). In agreement, we showed previously by means of filter retardation assays that WO1 selectively detects different protein fibrillation states in the nucleus [Arnhold and von Mikecz, 2011].

The property of I-Hg to induce intracellular protein aggregation was confirmed *in vivo*, *e.g.* in adult hermaphrodite *C. elegans* nematodes. Worms were left untreated or exposed to 60 µM I-Hg for 24 hours (Supplemental Fig. S3) and stained for amyloid-formation by means of the amyloid-specific dye Congo red. While untreated worms show a weak staining, a discontinuous, high-intensity pattern indicating protein fibrillation is observed in I-Hg-exposed *C. elegans* (Supplemental Fig. S3). These

Congo red binding domains are localized in the cell nucleus, especially in nucleoli and at the nuclear rim.

Heavy metal-induced protein fibrillation has been previously reported for (i) lead and Aβ [Basha et al., 2005], (ii) aluminum, iron, cobalt or copper and α-synuclein [Uversky et al., 2001] and (iii) mercury and Tau [Yang et al., 2010]. Our results indicate that endogenous nuclear proteins likewise have the propensity to aggregate into higher order amyloid-like conformations. Measurement of intracellular (total) Hg by means of atomic absorption spectroscopy (AAS) shows that the heavy metal concentrates in the nucleus (Table 1) which enables direct interactions between Hg-ions and nuclear proteins. The detection of nuclear amyloid in a physiological ground state as well as under conditions of mild I-Hg-exposition raises the question about functional versus adverse, *i.e.* pathogenic, roles of nuclear protein fibrillation. Here, identification of the nuclear proteins that undergo protein fibrillation and become components of amyloid-like microenvironments may lead to a better understanding.

Protein composition of I-Hg-induced aggregates

We next asked how to identify components of amyloid-like nuclear protein aggregates and chose a filter assay developed by Scherzinger et al. [Scherzinger et al., 1997]. The filter retardation assay traps SDS-insoluble protein aggregates on cellulose acetate filters, whereas soluble proteins pass through the 0.2 µm sized pores. In order to distinguish single components of nuclear protein aggregates we eluted the retained protein fraction from the filters and characterized the proteins in an unbiased approach by mass spectrometry (Fig. 2G). Mass spectrometry of SDS-insoluble protein aggregates was performed as detailed in the Methods section. HEp-2 cells that were left untreated have a ground state aggregome that contains 14 proteins with mainly cytoskeletal or chromatin-organizing functions (Fig. 2H; Supplemental Table S1). After four hours of exposition to I-Hg the

number of SDS-resistant aggregate components increases to a total of 69 (Fig. 2H). Among these, 55 proteins represent specifically induced aggregate components that are mainly nuclear and involved in organization of chromatin and gene expression (Supplemental Table S1). In order to validate the results in neural cells the analysis of SDS-resistant aggregate components by mass spectrometry was replicated in differentiated, post-mitotic SH-SY5Y cells (Fig. 2H; Supplemental Table S2). In contrast to HEp-2 cells the ground state aggregome of SH-SY5Y neurons already consists of 33 proteins that are predominately nuclear and participate in chromatin organization or RNA processing. Induction of protein fibrillation by I-Hg results in an aggregome consisting of 76 proteins in total, from which 43 proteins are specifically recruited to the SDS-resistant protein fraction (Fig. 2H; Supplemental Table S2).

To validate the MS analysis filter retardation assays and subsequent immunoblotting were performed with representative candidates (Supplemental Fig. S4). All candidates that specifically occur in the induced aggregome likewise showed an increased signal, *i.e.* were trapped on cellulose acetate filters after induction of protein fibrillation in neural SH-SY5Y by I-Hg. In contrast, beta tubulin is present in both the ground state and the induced aggregome and is retained in the filter assays of ground state as well as I-Hg-treated SH-SY5Y, respectively (Supplemental Fig. S4A, top). To monitor protein aggregation the mouse monoclonal antibody 1C2 against a linear and extended conformation of polyQ repeats [Klein et al., 2013] was used showing that endogenous CAG-repeat proteins are recruited to I-Hg-induced protein aggregates (Supplemental Fig. S4A, bottom). In order to exclude increased gene expression of representative candidates as a cause for their increased retardation on the filters respective immunoblot analyses of the total cell fractions were carried out. Supplemetal Fig. S4B shows that representative aggregome components are equally expressed in total cell fractions of both fibrillation states, namely ground state and I-Hg-induced SH-SY5Y neurons corroborating the specificity of the filter trap results.

Additional confirmation of single candidates comes from aggregomes that were previously characterized using (over)expression of ectopic amyloid proteins to analyze their interactions with the endogenous proteome. A study that reports induction of protein aggregation by expression of ectopic, EGFP-fused, CAG-expanded (Q150) huntingtin exon1 in murine Neuro2A cells shows that the RNA-binding protein FUS is a major component of nuclear polyQ aggregates [Doi et al., 2008]. Notably, FUS is likewise a component of I-Hg-induced nuclear protein aggregates in both cell types HEp-2 and SH-SY5Y. Lamin B1 and the AAA^+ ATPase ruvB-like 1 that both are recruited to the I-Hg-induced aggregome were previously identified as interacting with artificial β sheet proteins [Olzscha et al., 2011], corroborating the participation of these candidates in processes of intracellular protein fibrillation.

In line with this is the biological replication, *i.e.* comparison of the ground state and I-Hg-induced aggregome in proliferating HEp-2 with neural SH-SY5Y cells. Respective results are summarized in a Venn diagram showing that the total number of exclusive ground state and I-Hg-induced aggregate components is similar in HEp-2 (n=69) and SH-SY5Y (n=76) cells (Fig. 2H). However, both cell lines differ concerning the intersection between ground state and I-Hg-induced state. In SH-SY5Y neurons the number of aggregate components that overlap between the ground state and I-Hg-induced aggregome is nearly threefold compared with HEp-2, *i.e.* 30 versus 12 proteins (Fig. 2H). Thus, studies of single aggregome components are required to identify patterns of protein fibrillation that indicate respective pathways.

Consistent with this idea, ubiquitin occurs as a unique component of the endogenous aggregome in I-Hg-induced SH-SY5Y neurons (Supplemental Table S2). The fact that ubiquitin likewise constitutes a diagnostic component of neural nuclear inclusions in brains of patients with triplet (CAG) repeat diseases [Ross and Poirier, 2004] corroborates I-Hg-induced SH-SY5Y neurons as a valid model for the characterization of protein fibrillation pathways in the cell nucleus and suggests involvement of the ubiquitin-proteasome system. The presence of heat shock proteins in the

I-Hg-induced HEp-2 and SH-SY5Y aggregomes and ubiquitin in the I-Hg-induced SH-SY5Y aggregome (Supplemetal Tables S1 and S2) as well as previous results demonstrating degradation of spliceosomal components U1-70k, SmB/B' and splicing factor SC35 by the ubiquitin-proteasome system [Rockel et al., 2005] prompted us to investigate if amyloid-like microenvironments in the nucleoplasm contain components of the ubiquitin-proteasome system or respective proteolytic activity. Confocal immunofluorescence double labelling shows colocalization of WO1-positive amyloid speckles with 20S proteasomes (Supplemental Fig. S5B, yellow, filled arrowhead). The respective line scans indicate nearly perfect colocalization (Supplemental Fig. S5B, open arrowhead) suggesting that amyloid speckles recruit proteasomes and may represent proteolytic centers. Consistent with this idea analysis of global proteasomal activity indicated that I-Hg-induced protein fibrillation specifically activates the nuclear ubiquitin-proteasome system ($p<0.05$) (Supplemental Fig. S6B), probably to counteract further protein aggregation and maintain protein homeostasis in the nucleus. Formation of amyloid-like nuclear inclusions that contain proteolytic activity was shown previously after exposition of cells with another xenobiotic, namely silica nanoparticles [Chen et al., 2008]. A significant subpopulation (30%) of silica-nanoparticle-induced amyloid-like inclusions were identified as proteolytically active supporting the idea that amyloid-domains in the nucleus represent sites of proteasomal protein degradation.

Overrepresentation of cross-links and protein interactions in components of nuclear protein aggregates

We next searched for unifying protein sequence features of the aggregome components that were identified by mass spectrometry. For this purpose the presence of selected features in aggregated proteins were quantified and compared to the mean value of all database-saved proteins (database reference). This analysis shows a two to three fold higher presence of beta strands and

helix structures in aggregated proteins compared with statistical expectations from the average protein population (Fig. 3A). Especially cross-links stand out with an up to 20 fold overrepresentation. Up to two fold overrepresentation was observed for DNA- and nucleotide binding as well as for sequence repeats. In contrast, zinc finger structures and disulfide(SH)-bonds are underrepresented which refutes the assumption that treatment with I-Hg induces random protein aggregation by its affinity to SH-groups and argues for isopeptide bonds as likely constituents of the overrepresented cross-links. Surprisingly, coiled coil structures, which are intrinsically aggregation-prone [Fiumara et al., 2010], are underrepresented in aggregome components. In summary, SDS-insoluble aggregome components mainly differ from the global proteome concerning cross links that are even more enriched in the ground state of protein fibrillation (Fig. 3A). In order to investigate whether only the presence or the quantity of a feature within a protein is characteristic for aggregome components, the number of respective features within one protein was extracted from the database and compared with the global proteome (Supplemental Fig. S7A). The results suggest that the mere presence of a specific protein structure or sequence feature is characteristic for aggregated proteins irrespective of the quantity of the feature within each single protein.

The analysis of protein features indicates a statistically elevated chance that aggregated proteins have cross-links, β strands and helices as well as nucleotide-binding capability in comparison with other cellular proteins. These features are important for protein-protein interactions and formation of multi-protein complexes. Therefore, we next investigated the interaction propensity of the candidates identified by mass spectrometry. To this end database-listed interaction partners of each aggregate component (compare Supplemental Tables S1 and S2) were quantified, pooled and presented as box plots. All aggregate components show a median value of 60 to 100 known interaction partners per protein with a few extreme values that reach up to 3000 partners (Fig. 3B). Thus, aggregate components interact more frequently in comparison with the whole protein population listed in the database that has a median value of only eight interaction partners per protein. The non-

parametric Mann-Whitney test shows that proteins of the I-Hg-induced aggregome have a significantly higher number of interaction partners (Fig. 3B; $p<0.05$). This supports the idea that aggregate components are proteins with elevated structural interaction capabilities and propensity for complex formation, have a higher number of interaction partners and are therefore prone to form insoluble aggregates. It is tempting to speculate that a certain threshold of protein aggregation might already occur in the ground state of the cell as a functional feature of intracellular crowding and protein homeostasis, however may affect more and different proteins under cellular stress, *i.e.* if proteostasis is altered by I-Hg (Supplemental Fig. S5 and S6). Highly structured aggregate components that have many protein interaction partners are likely constituents of multi-protein complexes and contributors to overcrowded microenvironments and protein fibrillation.

Overrepresentation of nuclear proteins in protein aggregates

Next the subcellular localization of I-Hg-induced aggregome components was analyzed. Proteins were defined according to the database UniProtKB in three categories as located in the nucleus or in the cytoplasm or localized in both nucleus and cytoplasm. In ground state HEp-2 42.9% nuclear and 42.9% cytoplasmic aggregome components distribute equally within the two compartments, whereas a subpopulation of 14.2% proteins are both nuclear and cytoplasmic (Fig. 3C). After induction of protein fibrillation by I-Hg the percentage of nuclear proteins and cytoplasmic proteins is decreased to 38.2% and 32.7%, respectively, while aggregome components that occur in the nucleus as well as in the cytoplasm increase to 29.1% (Fig. 3C'). Neural SH-SY5Y cells have a clear predominance of nuclear aggregome components in both fibrillation states, *i.e.* 57.6% in ground state and 51.2% in the I-Hg-induced state (Fig. 3, D and D'). The overrepresentation of nuclear proteins in all examined aggregomes clearly shows when protein location is compared with the complete UniProtKB database where only 21.9% of the proteins are nuclear, 65.0% are cytoplasmic

528 and 13.0% are defined as occurring in both cellular compartments (Fig. 3E). These results indicate
529 that the nucleus is a major target for protein aggregation. Nuclear characteristics such as protein
530 crowding [Munishkina et al., 2008; Hancock, 2014] and organization into domains of concentrated
531 chromatin, molecular machines and ribonucleoprotein complexes [Rouquette et al., 2010; Hemmerich
532 et al., 2011] may contribute to the facilitated formation of SDS-resistant protein aggregates and
533 amyloidogenic microenvironments (Fig. 2, A-F), respectively.

534

535 **Spliceosomal components are a major constituent of I-Hg-induced protein aggregates**

536 A PANTHER databank analysis was performed in order to group proteins of the I-Hg-induced
537 aggregome according to their molecular and cellular function. In Fig. 3F aggregome components are
538 assigned to molecular and cellular functions, *i.e.* PANTHER classes, showing that in ground state
539 HEp-2 cells protein aggregation is restricted to chromatin-binding proteins, mainly histones,
540 intermediate filaments and other cytoskeletal proteins (Fig. 3F, first column, grey bars). After induction
541 of an advanced protein fibrillation state by I-Hg the aggregome additionally contains proteins involved
542 in RNA processing, chaperones, nucleoskeleton, a transcriptional cofactor and a variety of enzymes
543 (Fig. 3F, first column, black bars). With 27 proteins the RNA processing factors constitute the largest
544 functional group of the I-Hg-induced aggregome.

545 A similar distribution of functional classes is observable in neural SH-SY5Y cells. The
546 prevalence of RNA processing factors and chaperones occurs in both fibrillation steps, *e.g.* ground
547 and I-Hg-induced state (Fig. 3F, second column, gray or black bars, respectively). In contrast to HEp-2
548 cells transcriptional coactivators are a functional class that is specifically induced in SH-SY5Y neurons.
549 With 16 proteins in ground state and 19 proteins in the I-Hg-induced fibrillation state RNA processing
550 factors again stand out as the largest functional class corroborating the results obtained from I-Hg-
551 induced HEp-2 cells. This functional class contains spliceosomal components such as heterogeneous

552 ribonucleoprotein particles (hnRNPs), serine/arginine rich (SR) proteins, splicing factors and RNA
553 helicases that participate in a variety of splicing complexes and processes. Thus, processing and
554 maturation of RNA is identified as a major target of I-Hg- induced protein aggregation in the nucleus
555 which raises the question of interactions between nuclear protein fibrillation and splicing. Notably, the
556 nucleoskeletal protein lamin B1 is a constituent of both I-Hg-induced aggregomes, *e.g.* in HEp-2 and
557 SH-SY5Y cells.

558

559 **Data bank analysis of spliceosomal aggregate components**

560 Next we used the spliceosome database [Cvitkovic and Jurica, 2013] for detailed
561 characterization of the I-Hg-aggregome candidates that belong to the functional class of RNA
562 processing factors. Table 2 lists aggregome components from HEp-2 cells and SH-SY5Y neurons in
563 ground state or I-Hg-induced fibrillation states with respect to their molecular weight, class / family and
564 participation in different spliceosomal complexes. Splicing occurs as a cascade of subsequent steps
565 that are performed by spliceosomal E, A, B, B* and C complexes [Wahl et al., 2009]. These
566 complexes contain small nuclear ribonucleoproteins (snRNP) and non-snRNP proteins that assemble
567 stepwise on pre-mRNA and undergo major structural rearrangements during the process. Previous
568 MS analyses of spliceosomal complexes indicated that single spliceosomal assembly intermediates
569 consist of 150 to 300 proteins [Zhou et al., 2002].

570 Our data base analysis of the aggregome components belonging to the PANTHER class of
571 RNA processing shows that they are represented in all families / classes of spliceosome-associated
572 proteins and cover all steps of the splicing cascade (Table 2). In ground state HEp-2 cells we did not
573 detect any SDS-insoluble aggregated spliceosomal components, whereas the I-Hg-induced HEp-2
574 aggregome recruits spliceosomal components from all families / classes except hnRNP / U2snRNP,
575 alternative splicing factors, and mRNA binding proteins (Table 2). While the neural SH-SY5Y ground

state aggregome harbors a repertoire of splicing-associated proteins that participate in a reduced subset of families / classes, the I-Hg-induced fibrillation state recruits spliceosomal components from all families except hnRNP / U2snRNP and SR proteins. This represents a notable switch between ground state and I-Hg-induced protein fibrillation in SH-SY5Y, since in the ground state hnRNP/ U2snRNP and SR proteins participate in the SDS-insoluble aggregome (Table 2).

Consistent with this new questions emerge. What does I-Hg-induced aggregation of certain subsets of spliceosomal components imply for the delicate and complex splicing network? Are single spliceosomal components with key roles in the formation of RNA / RNP structures and / or catalysts of splicing segregated in I-Hg-induced nuclear amyloid? Key components of RNA processing such as the RNA helicases are essential for spliceosomal RNA-RNA rearrangements or RNP remodeling events [Staley and Guthrie, 1998] and thus amyloid fibrillation of these proteins might induce altered splicing. Consistently, the aggregomes identified in this study may represent snap shots of ongoing splicing processes, *i.e.* their modification.

Spliceosomal components colocalize with nuclear amyloid

A prerequisite for protein-protein interactions is their subcellular localization. In order to investigate the location of I-Hg-induced nuclear amyloid in correlation to spliceosomes confocal immunofluorescence was performed with antibodies that detect amyloid structures (Fig. 4, A-B', WO1, green) and human antibodies that recognize spliceosomal components, *i.e.* U1-70k RNPs and Sm proteins (Fig. 4, A-B', red). Confocal imaging shows that in ground state HEp-2 cells nuclear distribution of WO1 mainly occurs in nucleoli, whereas spliceosomal components U1-70K and Sm are distributed throughout the nucleoplasm and enriched in reticulated speckles (Fig. 4A, inset; compare with Fig. 2A). The respective line scan confirms that there is no overlap between amyloid structures in nucleoli and nucleoplasmic speckles. In an advanced fibrillation state, *e.g.* after induction with I-Hg,

amyloid structures are not confined to nucleoli, but likewise occur in the nucleoplasm where they partially colocalize with spliceosomal components in reticulated speckles (Fig. 4B, inset, filled arrowhead, yellow). Colocalization of WO1 and U1-70k / SmB antibodies is depicted in the corresponding line scan (open arrowhead). The imaging results showing amyloid-like microenvironments in speckles enriched with spliceosomal components in I-Hg-treated HEp-2 cells (Fig. 4B, yellow) confirm mass spectrometry that identifies RNA processing factors as the major entity of the endogenous aggregome in an advanced fibrillation state due to the heavy metal Hg. Thus, in HEp-2 cells two fibrillation states are characterized by a transition from a ground state without detectable amyloid to an induced state where amyloid-like aggregation of spliceosomal components occurs in distinct microenvironments in the center (core) of nuclear speckles (Fig. 4B', 3D reconstruction, z-axis views).

To investigate different protein fibrillation steps in correlation with RNA processing of specific targets the ratio between the splice variants of lamin A/C was monitored in untreated and I-Hg-treated cells (Fig. 4C). Alternative splicing of the human *lmna* gene in exon 10 eventually gives rise to lamin A (69 kD) or lamin C (62kD) proteins [Lin and Worman, 1993]. Immunoblotting shows that induction of protein fibrillation by I-Hg is correlated with a significant reduction of lamin A expression by 20% ($p<0.05$), whereas expression of lamin C remains unchanged (Fig. 4C, bar graph). This is consistent with the idea that amyloid fibrillation in nucleoplasmic microenvironments may modulate gene expression, here at the level of mRNA splicing.

Nucleoskeletal protein lamin B1 regulates formation of speckles enriched with spliceosomal components and amyloid-like microenvironments.

To understand the mechanism of the formation of amyloid-like microenvironments the I-Hg-aggregome component lamin B1 was selected for further investigations due to its participation in the

nucleoskeleton [Simon and Wilson, 2011] and previously reported interactions with nuclear speckles enriched with spliceosomal components [von Mikecz et al., 1997; Tang et al., 2008]. HEp-2 cells were transfected with respective small interfering (si) RNAs in different concentrations to specifically knock down expression of lamin B1 (specificity of RNAi is shown in Supplemental Fig. S8). By confocal immunofluorescence we observed in lamin B1 siRNA-treated cells a decrease of lamin B1 labelling at the nuclear envelope and in the nucleoplasm (Fig. 5A; green) as well as a reduced number of speckles enriched with spliceosomal components (Fig. 5, A and C; red). This correlation between lamin B1 knock down and speckle formation was observed in untreated and I-Hg-treated cells, *i.e.* correlated with ground state as well as I-Hg-induced protein fibrillation (Supplemental Fig. S9; Supplemental Table S3).

RNAi experiments likewise demonstrate a correlation between reduction of lamin B1 expression and formation of Congo red-binding microenvironments that indicate nuclear amyloid (Fig. 5B). However, this correlation is particularly observed in I-Hg-treated cells (Fig. 5, D-F; Supplemental Fig. S9; Supplemental Table S4) suggesting that lamin B1 specifically sustains formation of amyloid-like microenvironments in the cell nucleus as part of the I-Hg-induced aggregome network (Supplemental Table S1). This is consistent with the current view that lamin B1 forms a distinct filament network in living nuclei supporting nuclear processes such as transcription, replication and chromatin organization [Shimi et al., 2008; Simon and Wilson, 2011]. Here, we introduce the idea that lamin B1 likewise regulates nuclear protein fibrillation, *i.e.* formation of nuclear amyloid.

CONCLUSIONS

The present study identifies lamin B1-dependent amyloid formation in the cell nucleus as a novel bio-interaction of the global pollutant Hg. Similar to protein aggregation events in the cytoplasm that are controlled by the cytoskeleton [Kopito, 2000], the counterpart in the nucleus, *e.g.* amyloid

fibrillation of nuclear proteins, may be driven by the nucleoskeleton. Characterization of the I-Hg-induced protein aggregation landscape reveals the nucleus as a major target of stepwise protein fibrillation that peaks with formation of amyloid microdomains in the core of speckles enriched with spliceosomal components. While substructures such as PML and Cajal nuclear bodies have previously been connected to neural nuclear inclusions in patients with CAG-repeat diseases and respective mouse models [Davies et al., 1997; von Mikecz, 2014], speckles enriched with RNA processing factors are defined here as amyloidogenic venues and prevalent components of an endogenous aggregome for the first time. A notable similarity between transitional steps of amyloid fibrillation and formation of different spliceosomal complexes in the splicing cascade is partial structural unfolding of their protein components [Coelho Ribeiro Mde et al., 2013; Uversky, 2014]. This similarity may explain the aggregation propensity of spliceosomal components and our observation of I-Hg-induced amyloid speckles. In fact, aggregome components such as FUS, hnRNPA1 or hnRNPA2/B1 contain prion like-domains with high prion scores, *i.e.* propensity for prion formation [Li et al., 2013]. Accordingly, recruitment of FUS, hnRNPA1 and hnRNPA2/B1 to cytoplasmic stress granules was observed *in vitro* and in a subpopulation of patients with the progressive neurodegenerative disease amyotrophic lateral sclerosis (ALS) [Kim et al., 2013; Li et al., 2013]. Although we do not detect accumulation of FUS or hnRNPs in cytoplasmic stress granules after I-Hg-treatment (data not shown) these proteins clearly are prone to undergo fibrillation in distinct subcellular domains that may depend on environmental conditions and the degree of protein fibrillation.

Components of the I-Hg-induced aggregome such as lamin B1, ubiquitin, heat shock protein HSP70 and spliceosomal aggregate components clearly participate in a framework of aberrant protein aggregation pathways in the nucleus. By identification of this aggregome network we have just started to elucidate the interplay between nuclear protein homeostasis and I-Hg-induced impairment of neural function, *e.g.* neurotoxicity. As the extent of anthropogenic Hg release is becoming increasingly evident due to advanced global monitoring [Lamborg et al., 2014] and I-Hg rises in the US population

673 in an age-dependent manner [Laks, 2014], our work urges further investigation of Hg-amyloid
674 interactions in cross-species studies and translation of the results to epidemiologic data.

675

677 AUTHOR CONTRIBUTIONS

678 AvM conceived the study. FA performed the majority of the experiments. KHG performed mass

679 spectrometry. FA and AvM did the data analysis. FA, KHG and AvM contributed to manuscript

680 preparation. FA and AvM wrote the manuscript. AvM acquired funding.

681

683 ACKNOWLEDGEMENTS

684 We thank Burkhardt Dahlmann and Ronald Wetzel for donation of antibodies, Jürgen Wittsiepe
685 for help with atomic absorption spectroscopy, and members of the von Mikecz laboratory for critical
686 discussions.

687

689 REFERENCES

690 Amos HM, Jacob DJ, Kocman D, Horowitz HM, Zhang Y, Dutkiewicz S, Horvat M, Corbitt ES,
691 Krabbenhoft DP, Sunderland EM. 2014. Global Biogeochemical Implications of Mercury Discharges
692 from Rivers and Sediment Burial. *Environ Sci Technol* **48**: 9514-9522

693 Arnhold F, von Mikecz A. 2011. Quantitative feature extraction reveals the status quo of protein
694 fibrillation in the cell nucleus. *Integr Biol* (Camb) **3**: 761-769

695 Axelrad DA, Bellinger DC, Ryan LM, Woodruff TJ. 2007. Dose-response relationship of prenatal
696 mercury exposure and IQ: an integrative analysis of epidemiologic data. *Environ Health Perspect* **115**:
697 609-615

698 Basha MR, Murali M, Siddiqi HK, Ghosal K, Siddiqi OK, Lashuel HA, Ge YW, Lahiri DK, Zawia NH.
699 2005. Lead (Pb) exposure and its effect on APP proteolysis and Aβ aggregation. *FASEB J* **19**: 2083-
700 2084

701 Bocharova N, Treu G, Czirják GÁ, Krone O, Stefanski V, Wibbelt G, Unnsteinsdóttir ER, Hersteinsson
702 P, Schares G, Doronina L, Goltsman M, Greenwood AD. 2013. Correlates between feeding ecology
703 and mercury levels in historical and modern arctic foxes (Vulpes lagopus). *PLoS One* **8**: e60879

704 Brenner S. 1974. The genetics of *Caenorhabditis elegans*. *Genetics* **77**: 71-94

705 Chen M, Singer L, Scharf A, von Mikecz A. 2008. Nuclear polyglutamine-containing protein
706 aggregates as active proteolytic centers. *J Cell Biol* **180**: 697-704

707 Chiti F, Dobson CM. 2009. Amyloid formation by globular proteins under native conditions. *Nat Chem*
708 *Biol* **5**: 15-22

709 Clarkson TW, Magos L. 2006. The toxicology of mercury and its chemical compounds. *Crit Rev*
710 *Toxicol* **36**: 609-62

711 Coelho Ribeiro Mde L, Espinosa J, Islam S, Martinez O, Thanki JJ, Mazariegos S, Nguyen T, Larina
712 M, Xue B, Uversky VN. 2013. Malleable ribonucleoprotein machine: protein intrinsic disorder in the
713 Saccharomyces cerevisiae spliceosome. *PeerJ* **1**: e2

714 Cvitkovic I, Jurica MS. 2013. Spliceosome database: a tool for tracking components of the
715 spliceosome. *Nucleic Acids Res* **41**: D132-141

716 Davies SW, Turmaine M, Cozens BA, DiFiglia M, Sharp AH, Ross CA, Scherzinger E, Wanker EE,
717 Mangiarini L, Bates GP. 1997. Formation of neuronal intranuclear inclusions underlies the neurological
718 dysfunction in mice transgenic for the HD mutation. *Cell* **90**: 537-548

719 DiFiglia M, Sapp E, Chase KO, Davies SW, Bates GP, Vonsattel JP, Aronin N. 1997. Aggregation of
720 huntingtin in neuronal intranuclear inclusions and dystrophic neurites in brain. *Science* **277**: 1990-
721 1993

722 Doi H, Okamura K, Bauer PO, Furukawa Y, Shimizu H, Kurosawa M, Machida Y, Miyazaki H, Mitsui
723 K, Kuroiwa Y, Nukina N. 2008. RNA-binding Protein TLS Is a Major Nuclear Aggregate-interacting
724 Protein in Huntingtin Exon 1 with Expanded Polyglutamine-expressing Cells. *J Biol Chem* **283**: 6489-
725 6500

726 Eto K. 1997. Pathology of Minamata disease. *Toxicol Pathol* **25**: 614-623

727 Fiumara F, Fioriti L, Kandel ER, Hendrickson WA. 2010. Essential role of coiled coils for aggregation
728 and activity of Q/N-rich prions and PolyQ proteins. *Cell* **143**: 1121-1135

729 Goedert M. 2001. Alpha-synuclein and neurodegenerative diseases. *Nat Rev Neurosci* **2**: 492-501

730 Grandjean P, Weihe P, Needham LL, Burse VW, Patterson DG Jr, Sampson EJ, Jørgensen PJ,
731 Vahter M. 1995. Relation of a seafood diet to mercury, selenium, arsenic, and polychlorinated
732 biphenyl and other organochlorine concentrations in human milk. *Environ Res* **71**: 29-38

733 Grandjean P, Weihe P, White RF, Debes F, Araki S, Yokoyama K, Murata K, Sørensen N, Dahl R,
734 Jørgensen PJ. 1997. Cognitive deficit in 7-year-old children with prenatal exposure to methylmercury.
735 *Neurotoxicol Teratol* **19**: 417-428

736 Hancock R. 2004. A role for macromolecular crowding effects in the assembly and function of
737 compartments in the nucleus. *J Struct Biol* **146**: 281-290

738 Hemmerich P, Schmiedeberg L, Diekmann S. 2011. Dynamic as well as stable protein interactions
739 contribute to genome function and maintenance. *Chromosome Res* **19**: 131-151

740 Ikemoto T, Kunito T, Watanabe I, Yasunaga G, Baba N, Miyazaki N, Petrov EA, Tanabe S. 2004.
741 Comparison of trace element accumulation in Baikal seals (*Pusa sibirica*), Caspian seals (*Pusa*
742 *caspica*) and northern fur seals (*Callorhinus ursinus*). *Environ Pollut* **127**: 83–97

743 Kim EY, Murakami T, Saeki K, Tatsukawa R. 1996. Mercury levels and its chemical form in tissues
744 and organs of seabirds. *Arch Environ Contam Toxicol* **30**: 259–266

745 Kim HJ, Kim NC, Wang YD, Scarborough EA, Moore J, Diaz Z, MacLea KS, Freibaum B, Li S, Molliex
746 A, Kanagaraj AP, Carter R, Boylan KB, Wojtas AM, Rademakers R, Pinkus JL, Greenberg SA,
747 Trojanowski JQ, Traynor BJ, Smith BN, Topp S, Gkazi AS, Miller J, Shaw CE, Kottlors M, Kirschner J,
748 Pestronk A, Li YR, Ford AF, Gitler AD, Benatar M, King OD, Kimonis VE, Ross ED, Weihl CC, Shorter
749 J, Taylor JP. 2013. Mutations in prion-like domains in hnRNPA2B1 and hnRNPA1 cause multisystem
750 proteinopathy and ALS. *Nature* **495**: 467-473

751 Klein FA, Zeder-Lutz G, Cousido-Siah A, Mitschler A, Katz A, Eberling P, Mandel JL, Podjarny A,
752 Trottier Y. 2013. Linear and extended: a common polyglutamine conformation recognized by the three
753 antibodies MW1, 1C2 and 3B5H10. *Hum Mol Genet* **22**: 4215-4223

754 Knowles TP, Vendruscolo M, Dobson CM. 2014. The amyloid state and its association with protein
755 misfolding diseases. *Nat Rev Mol Cell Biol* **15**: 384-396

756 Knudsen LB, Borgå K, Jørgensen EH, van Bavel B, Schlabach M, Verreault J, Gabrielsen GW. 2007.
757 Halogenated organic contaminants and mercury in northern fulmars (Fulmarus glacialis): levels,
758 relationships to dietary descriptors and blood to liver comparison. *Environ Pollut* **146**: 25-33

759 Kopito RR. 2000. Aggresomes, inclusion bodies and protein aggregation. *Trends Cell Biol* **10**: 524-530

760 Korbas M, O'Donoghue JL, Watson GE, Pickering IJ, Singh SP, Myers GJ, Clarkson TW, George GN.
761 2010. The chemical nature of mercury in human brain following poisoning or environmental exposure.
762 *ACS Chem Neurosci* **1**: 810-818

763 Laks DR. 2014. Mercury rising: response to the EPA assessment of mercury exposure. *Biometals* **27**:
764 1-4

765 Lamborg CH, Hammerschmidt CR, Bowman KL, Swarr GJ, Munson KM, Ohnemus DC, Lam PJ,
766 Heimbürger LE, Rijkenberg MJ, Saito MA. 2014. A global ocean inventory of anthropogenic mercury
767 based on water column measurements. *Nature* **512**: 65-68

768 Li YR, King OD, Shorter J, Gitler AD. 2013. Stress granules as crucibles of ALS pathogenesis. *J Cell*
769 *Biol* **201**: 361–372

770 Lin F, Worman HJ. 1993. Structural Organization of the Human Gene Encoding Nuclear Lamin A and
771 Nuclear Lamin C. *J Biol Chem* **268**: 16321-16326

772 Malinow R, Madison DV, Tsien RW. 1988. Persistent protein kinase activity underlying long-term
773 potentiation. *Nature* **335**: 820-824

774 Mi H, Muruganujan A, Thomas PD. 2013. PANTHER in 2013: modeling the evolution of gene function,
775 and other gene attributes, in the context of phylogenetic trees. *Nucleic Acids Res* **41**: D377-386

776 Munishkina LA, Ahmad A, Fink AL, Uversky VN. 2008. Guiding protein aggregation with
777 macromolecular crowding. *Biochemistry* **47**: 8993-9006

778 Olzscha H, Schermann SM, Woerner AC, Pinkert S, Hecht MH, Tartaglia GG, Vendruscolo M, Hayer-
779 Hartl M, Hartl FU, Vabulas RM. 2011. Amyloid-like Aggregates Sequester Numerous metastable
780 Proteins with Essential Cellular Functions. *Cell* **144**: 67-78

781 O'Nuallain B, Wetzel R. 2002. Conformational Abs recognizing a generic amyloid fibril epitope. *Proc*
782 *Natl Acad Sci USA* **99**: 1485-1490

783 Perez MK, Paulson HL, Pendse SJ, Saionz SJ, Bonini NM, Pittman RN. 1998. Recruitment and the
784 role of nuclear localization in polyglutamine-mediated aggregation. *J Cell Biol* **143**: 1457-1470

785 Rockel TD, Stuhlmann D, von Mikecz A. 2005. Proteasomes degrade proteins in focal subdomains of
786 the human cell nucleus. *J Cell Sci* **118**: 5231-5242

787 Ross CA, Poirier MA. 2004. Protein aggregation and neurodegenerative disease. *Nat Med* **10 Suppl**:
788 S10-17

789 Rouquette J, Cremer C, Cremer T, Fakan S. 2010. Functional nuclear architecture studied by
790 microscopy: present and future. *Int Rev Cell Mol Biol* **282**: 1-90

791 Schaefer MH, Fontaine JF, Vinayagam A, Porras P, Wanker EE, Andrade-Navarro MA. 2012. HIPPIE:
792 Integrating protein interaction networks with experiment based quality scores. *PLoS One* **7**: e31826

793 Scharf A, Piechulek A, von Mikecz A. 2013. Effect of nanoparticles on the biochemical and behavioral
794 aging phenotype of the nematode Caenorhabditis elegans. *ACS Nano* **7**: 10695-10703

795 Scherzinger E, Lurz R, Turmaine M, Mangiarini L, Hollenbach B, Hasenbank R, Bates GP, Davies
796 SW, Lehrach H, Wanker EE. 1997. Huntingtin-Encoded Polyglutamine Expansions Form Amyloid-like
797 Protein Aggregates In Vitro and In Vivo. *Cell* **90**: 549-558

798 Shimi T, Pfleghaar K, Kojima S, Pack CG, Solovei I, Goldman AE, Adam SA, Shumaker DK, Kinjo M,
799 Cremer T, Goldman RD. 2008. The A- and B-type nuclear lamin networks: microdomains involved in
800 chromatin organization and transcription. *Genes Dev* **22**: 3409-3421

801 Simon DN, Wilson KL. 2011. The nucleoskeleton as a genome-associated dynamic 'network of
802 networks'. *Nat Rev Mol Cell Biol* **12**: 695-708

Staley JP, Guthrie C. 1998. Mechanical devices of the spliceosome: motors, clocks, springs, and things. *Cell* **92**: 315-326

Streets DG, Devane MK, Lu Z, Bond TC, Sunderland EM, Jacob DJ. 2011. All-time releases of mercury to the atmosphere from human activities. *Environ Sci Technol* **45**: 10485-10491

Tang CW, Maya-Mendoza A, Martin C, Zeng K, Chen S, Feret D, Wilson SA, Jackson DA. 2008. The integrity of a lamin-B1-dependent nucleoskeleton is a fundamental determinant of RNA synthesis in human cells. *J Cell Sci* **121**: 1014-1024

UNEP. Global Mercury Assessment 2013: Sources, Emissions, Releases and Environmental Transport. (UNEP Chemicals Branch, Geneva, Switzerland, 2013)

Uversky VN. 2014. Introduction to Intrinsically Disordered Proteins (IDPs). *Chem Rev* **114**: 6557-6560

Uversky VN, Li J, Fink AL. 2001. Metal-triggered structural transformations, aggregation and fibrillation of human alpha-synuclein. A possible molecular NK between Parkinson's disease and heavy metal exposure. *J Biol Chem* **276**: 44284-44296

Vahter ME, Mottet NK, Friberg LT, Lind SB, Charleston JS, Burbacher TM. 1995. Demethylation of methyl mercury in different brain sites of Macaca fascicularis monkeys during long-term subclinical methyl mercury exposure. *Toxicol Appl Pharmacol* **134**: 273-284

von Mikecz A. 2014. Pathology and function of nuclear amyloid: Protein homeostasis matters. *Nucleus* **5**: 311-317

von Mikecz A, Konstantinov K, Buchwald DS, Gerace L, Tan EM. 1997. High frequency of autoantibodies to insoluble cellular antigens in patients with chronic fatigue syndrome. *Arthritis Rheum* **40**: 295-305

Wahl MC, Will CL, Lührmann R. 2009. The spliceosome: design principles of a dynamic RNP machine. *Cell* **136**: 701-718

Wanker EE, Scherzinger E, Heiser V, Sittler A, Eickhoff H, Lehrach H. 1999. Membrane filter assay for detection of amyloid-like polyglutamine-containing protein aggregates. *Methods Enzymol* **309**: 375-386

Wiesehan K, Buder K, Linke RP, Patt S, Stoldt M, Unger E, Schmitt B, Bucci E, Willbold D. 2003. Selection of D-amino-acid peptides that bind to Alzheimer's disease amyloid peptide abeta1-42 by mirror image phage display. *Chembiochem* **4**: 748-753

Wilhelm M, Wittsiepe J, Schrey P, Lajoie-Junge L, Busch V. 2003. Dietary intake of arsenic, mercury and selenium by children from a German North Sea island using duplicate portion sampling. *J Trace Elem Med Biol* **17**: 123-132

Yang DJ, Shuo S, Zheng LF, Yao TM, Ji LN. 2010. Mercury(II) Promotes the In Vitro Aggregation of Tau Fragment Corresponding to the Second Repeat of Microtubule-Binding Domain: Coordination and Conformational Transition. *Biopolymers* **93**: 1100-1107

Zhou Z, Licklider LJ, Gygi SP, Reed R. 2002. Comprehensive proteomic analysis of the human spliceosome. *Nature* **419**: 182-185

1

I-Hg reduces Ca2+-signalling in SH-SY5Y neurons.

Figure 1. I-Hg reduces Ca^{2+}-signalling in SH-SY5Y neurons. Intracellular Ca^{2+} of untreated or I-Hg-treated neural SH-SY5Y cells was monitored by the Fluo-4 DirectTM assay. Cells were imaged by time lapse confocal laser scanning microscopy with low resolution/ high speed settings. After 10 seconds cells were stimulated with either (A, B) KCl [75 mM] or with (C, D) the cholinergic agonist carbachol [0.1 µM]. (A, C) Intracellular fluorescence intensity of representative single cells was measured with MetaMorph software and plotted as intensity [a.u.] over time [s]. Continuous curve: untreated SH-SY5Y cells; dashed curve: I-Hg-treated SH-SY5Y cells. (B, D) Ca^{2+}-fluctuations were quantified by calculation of the intensity increase after stimulation as percentage (%) of the base line intensity. Results of three independent experiments were pooled and are presented as box plots (KCl/ w/o I-Hg, n = 312 cells; KCl/ + I-Hg, n = 291 cells; carbachol/ w/o I-Hg, n = 311 cells; carbachol/ + I-Hg, n = 301 cells). P-values of nonparametric Mann-Whitney tests indicate significant differences between untreated and I-Hg-treated cells. (E) Expression of T286-phosphorylated CaMKII and (F) total CaMKII was analyzed by immunoblotting. Untreated or I-Hg-exposed neural SH-SY5Y cells were either left unstimulated or additionally stimulated with KCl or carbachol. Bar graphs show mean values and standard deviations of densitometric analyses of three independent experiments. P-values ($p < 0.05$) indicate significant differences (one-way ANOVA with Tukey's post-hoc test). Corresponding Coomassie Brilliant Blue staining confirms equal protein loading. A.u., arbitrary units; s, seconds.

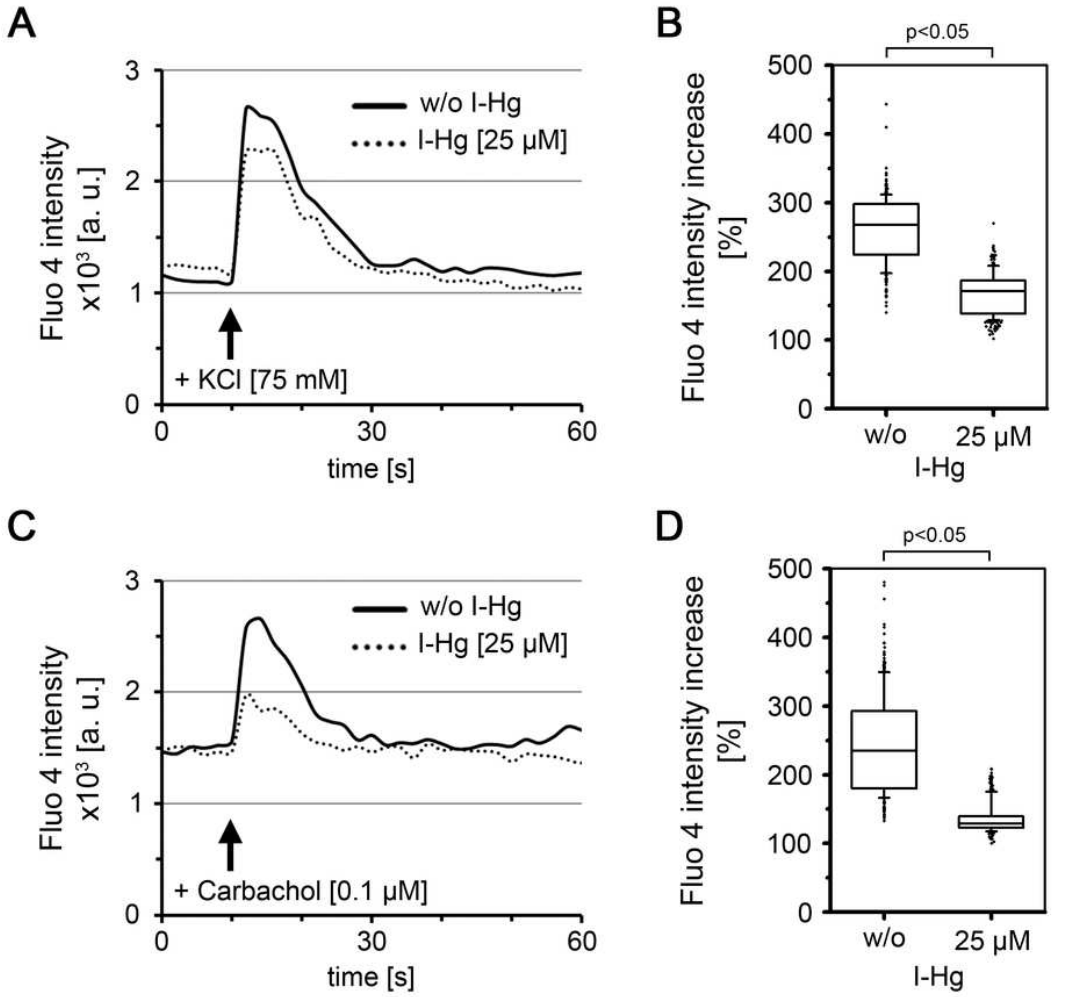

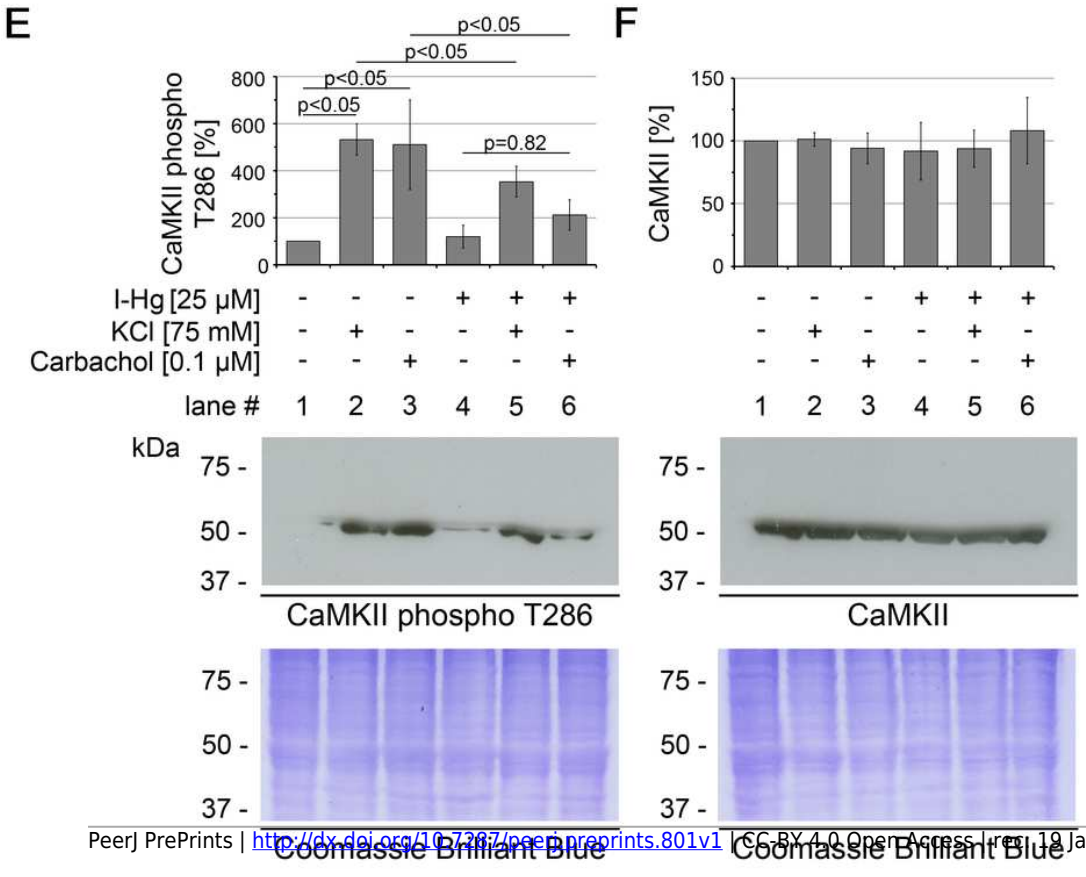

Mild concentrations of inorganic mercury increase local and global amyloid fibrillation in the cell.

Figure 2. Mild concentrations of inorganic mercury increase local and global amyloid fibrillation in the cell. Untreated or 4 hour I-Hg-treated HEp-2 cells were fixed and stained for intracellular amyloid. (A – F). Micrographs show confocal imaging of representative cells in differential interference contrast (DIC) or fluorescence channels. Blow ups show respective regions of the cell nucleus of the fluorescence channel visualized with pseudocolor (Metamorph) that indicates intensity of fluorescence (blue/green: low intensity, red/white: high intensity). Representative cells were immunolabelled with the amyloid-specific antibody WO1 and FITC-conjugated secondary antibodies w/o (A) or with I-Hg-exposure (B). Cells were stained with the amyloid dyes ThT (C, D) or CR (E, F). Note, the pattern change of the dyes in the nucleoplasm after induction of protein fibrillation by I-Hg (D, F). (G) Isolation and characterization of endogenous protein aggregates (schematic): human cells, *i.e.* proliferating HEp-2 or post-mitotic retinoic acid (RA)-differentiated, neural SH-SY5Y, were left untreated to investigate the ground state of protein aggregation or treated for 4 hours with I-Hg to induce an advanced step of endogenous protein fibrillation. Cells were lysed and SDS-insoluble protein aggregates isolated by filter retardation assays. Aggregates were eluted from the filters, re-suspended in 6M guanidinium-HCl and resulting samples analyzed by mass spectrometry (ESI-LC/MS). MS results were interpreted by means of proteomic, database-supported quantification. (H) The numbers of SDS-insoluble aggregate components in untreated and 4 hour I-Hg-treated HEp-2 cells or SH-SY5Y neurons are presented as Venn diagrams. Open sets represent the ground state of protein fibrillation, whereas hatched sets represent the induced fibrillation state. Respective intersections show aggregate components that coexist in ground and induced state aggregomes. Complete lists of candidates are available in Supplemental Tables S1 and S2. CR, Congo red; FITC, fluorescein isothiocyanate;

h, hours; I-Hg, inorganic mercury; RA, retinoic acid; ThT, Thioflavin T; w/o, without. Bar, 5 µm.

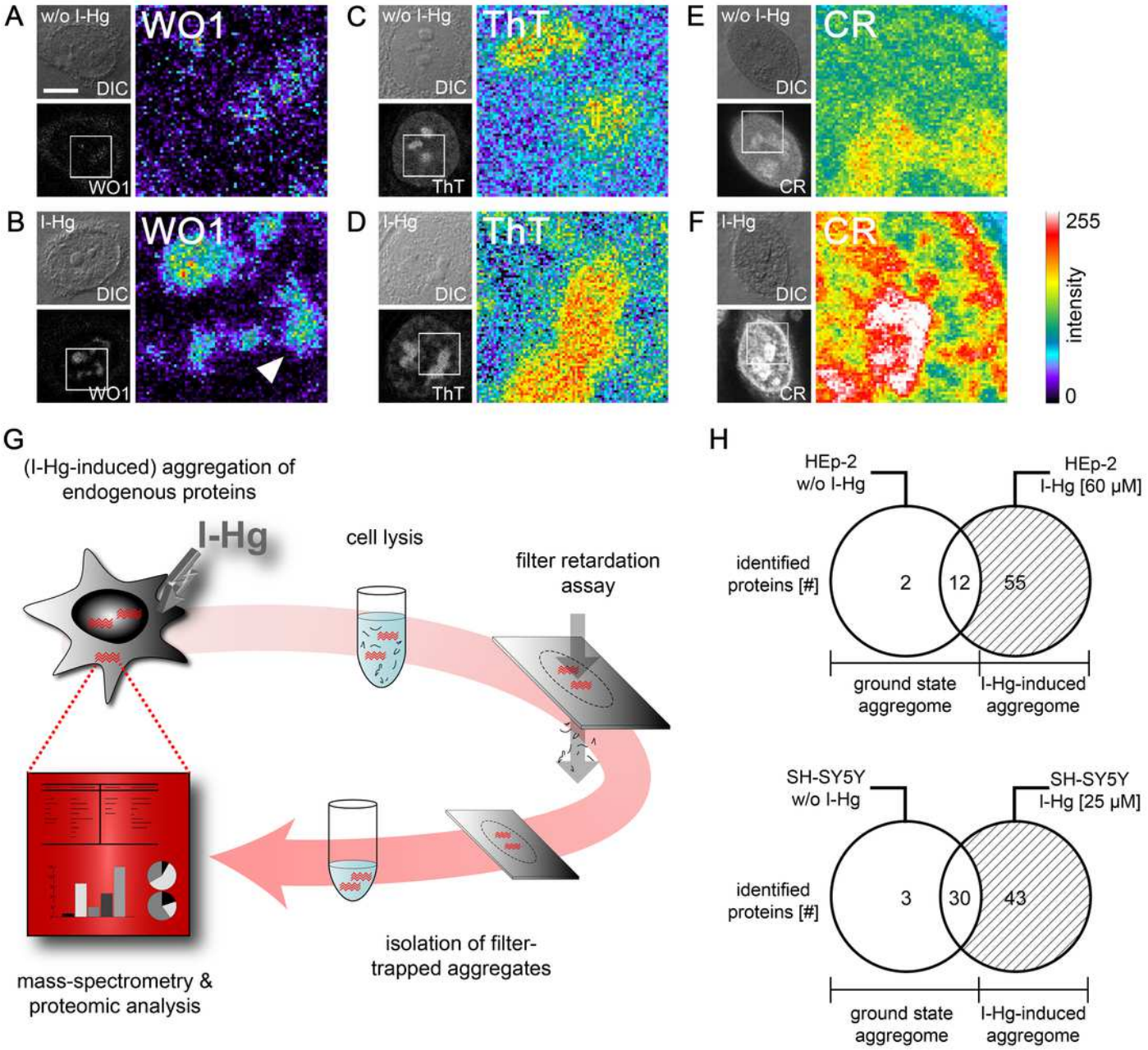

Aggregome components have a propensity for protein interactions and are mainly nuclear.

Figure 3. Aggregome components have a propensity for protein interactions and are mainly nuclear. Aggregated proteins show a statistical overrepresentation of cross-links (A) and a higher number of potential interaction partners (B) as compared to the complete proteome database. Sequence features were extracted from the UniProtKB database. Identified components of HEp-2 ground state (black), HEp-2 I-Hg-induced (grey), SH-SY5Y ground state (red) and SH-SY5Y I-Hg-induced (green) aggregates were analyzed. (A) The number of proteins with particular features [%] is calculated and presented as fold change to corresponding values of the complete human proteome database. The database reference line (y-value = 1) represents the value of a feature in the complete UniProtKB protein database. Corresponding values above 1 (upward bars) indicate statistical overrepresentation and values below 1 (downward bars) indicate underrepresentation. Values of features that are not found in a single sample (value = 0) are not depicted. (B) The HIPPIE database was used to calculate the number of potential interaction partners of aggregate components listed in Supplemental Tables S1 and S2. Pooled data is presented as box plots. Nonparametric Mann-Whitney test analyzes significant differences between different groups. p-values below 0.05 indicate significance. (C-E) The cell nucleus is a major target of protein aggregation. Parts c-d' show the subcellular location of proteins identified by mass spectrometry according to UniProtKB database entries. Data is calculated as percentage of each group and presented as pie charts for aggregate components of (C) HEp-2, ground state, (C') HEp-2, I-Hg-induced protein fibrillation state, (D) SH-SY5Y, ground state and (D') SH-SY5Y, I-Hg-induced protein fibrillation state, in comparison with (E) the complete UniProtKB protein database as reference. (F) shows classification of the identified proteins by application of the PANTHER database. The absolute numbers of proteins in each PANTHER

database protein class are depicted as bar graphs of HEp-2 cells or SH-SY5Y neurons (two pooled experiments per group; compare with Supplemental Tables S1 and S2). Analysis of aggregate components is subdivided into ground state (grey bars) or I-Hg-induced protein fibrillation (black bars). Where necessary, the original PANTHER class identifiers were modified and adjusted to the experimental data by manual customization.

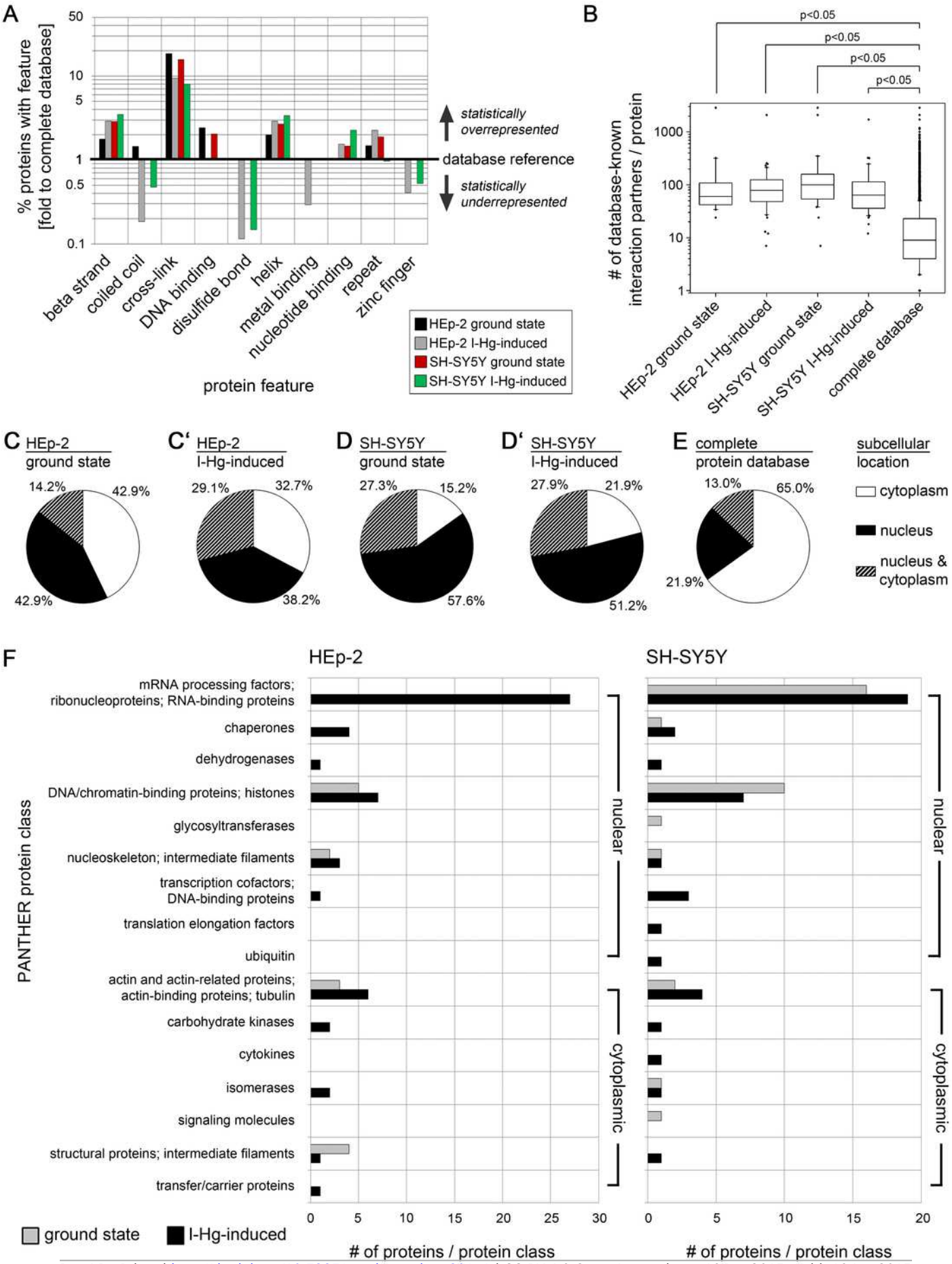

4

Amyloid-like microenvironments form in the center of nuclear speckles enriched with spliceosomal components.

Figure 4. Amyloid-like microenvironments form in the center of nuclear speckles enriched with spliceosomal components. (A) Confocal immunofluorescence of WO1 (green) and spliceosomal components (human autoimmune serum against U1-70k and Sm-proteins, red) shows partial colocalization after (B) 4 hours of I-Hg-treatment (merge, blow up). Separation or colocalization of WO1 and spliceosomal components is visualized by the linescan function of MetaMorph: the fluorescence intensity of each pixel of the line of interest (insets, asterisks, white lines) is shown as a xy-graph for the corresponding green and red channels. Arrows indicate nucleolar WO1-staining (green), whereas arrowheads indicate WO1-positive amyloid-like microenvironments in the nucleoplasm that colocalize with spliceosomal components (yellow). (B') A z-scan of the cell shown in (B) indicates central positioning of WO1-labelled amyloid-like microenvironments within nuclear speckles. Confocal xy-planes of the z-stack were 3D-reconstructed by MetaMorph (B', left). The same cell is shown by z-axis plane views along the indicated white lines, i.e. from the side and from below (B', middle). Three exemplary aggregates are presented as blow ups of the z-axis-views (B', right, insets 1-3). (C) shows a representative immunoblot of alternative splicing products lamin A/C in untreated (-) or I-Hg-treated (+) HEp-2 cells. Respective staining with the acid dye Coomassie brilliant blue indicates equal loading. The detected signals for lamin A/C were quantified by densitometric analysis, *i.e.* region of interest measurement using the software MetaMorph, and provided as mean values and standard deviations of three independent experiments. The values were normalized to the corresponding signal of untreated samples. A p-value < 0.05 indicates a statistical significant difference (tested with Student's t-test). A.u., arbitrary units; cy, cytoplasm; DIC, differential interference contrast; h, hours; ne, nuclear envelope; no, nucleolus; nu, nucleus. Bars, 5 µm.

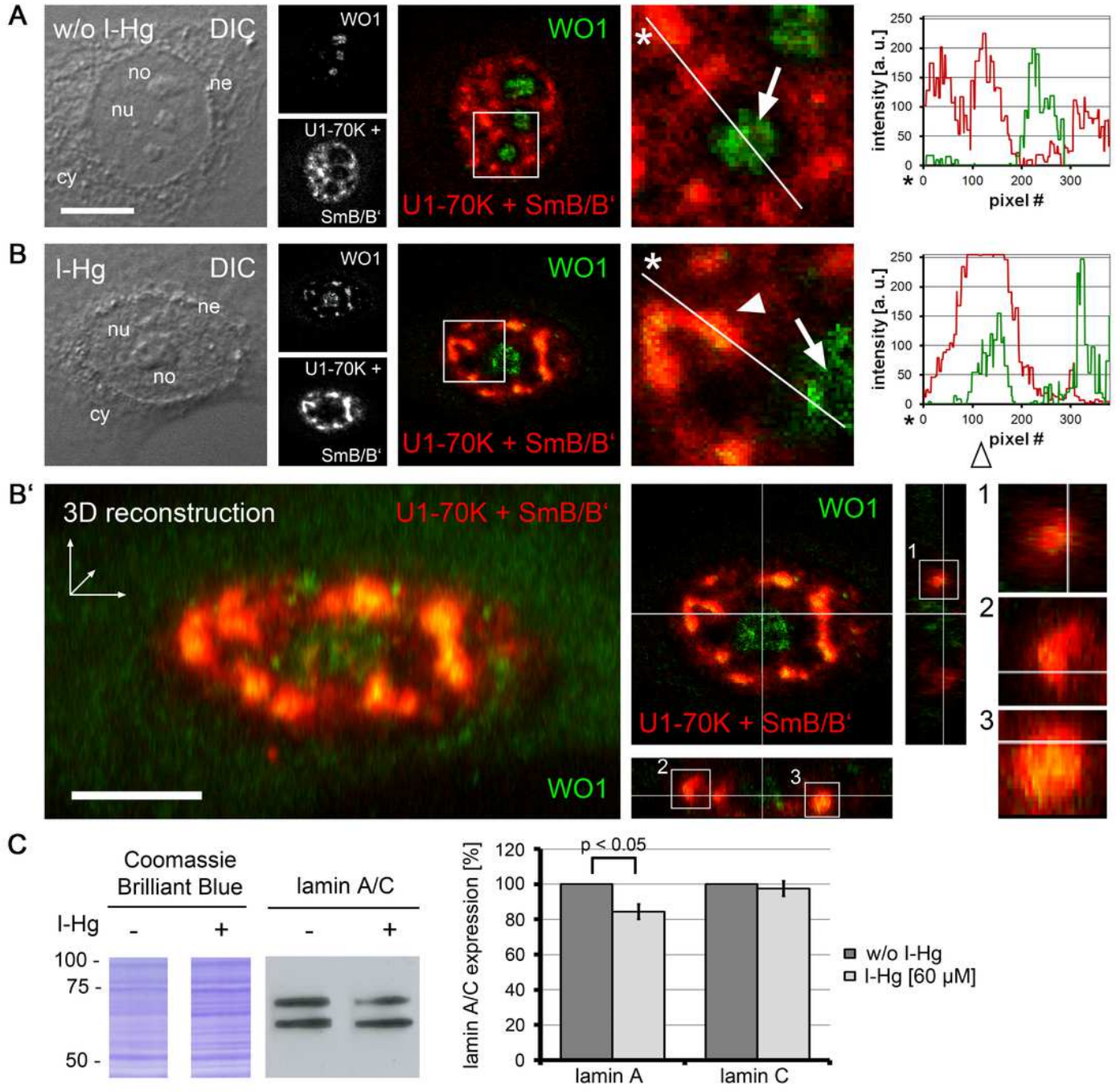

Nucleoskeletal protein lamin B1 regulates formation of I-Hg-induced nuclear amyloid.

Figure 5. Nucleoskeletal protein lamin B1 regulates formation of I-Hg-induced nuclear amyloid. Increasing concentrations of short interfering RNAs (siRNAs, 30 pmol and 60 pmol) were used to deplete lamin B1 in untreated or I-Hg-treated HEp-2 cells. Reduced lamin B1 expression was confirmed by immunoblotting (Supplemental Fig. S8). Controls include untreated or HEp-2 cells treated with scrambled, random siRNA (siRNA scr.). Cells were double-immunolabelled for lamin B1 and splicing components U1-70K/SmB/B'. (A) shows representative DICs of HEp-2 cells (top row) and indicated blow ups of respective nuclear envelope or nucleoplasmic regions with labelled lamin B1 (green) and U1-70K/SmB/B' (red) in single fluorescence channels and merge. Yellow staining indicates colocalization of nucleoplasmic lamin B1 and nuclear speckles enriched with splicing components. (B) To investigate influence of lamin B1 depletion on amyloid formation, untreated or I-Hg-treated HEp-2 cells were stained for Congo red-positive microenvironments. Representative cells are shown in DIC and fluorescence channels (*i.e.* pseudocolored micrographs). Bars, 5 µm. (C) Immunostained nuclear speckles enriched with spliceosomal components were quantified using the Integrated Morphometry Analysis tool in Metamorph. Nuclear speckles were detected by intensity threshold and analysed for (i) average number of speckles per nucleus, (ii) average speckle size as [a. u.] and (iii) average speckle shape (shape factor = 1: round; shape factor < 1: reticulated). (D) shows quantification of the nuclear Congo red fluorescence pattern, as described previously (Arnhold et al., 2011). The parameters for (i) Congo red pattern heterogeneity [a. u.], (ii) Congo red pattern intensity [a. u.] and (iii) nucleus area with Congo red positive aggregates [%] were used to quantitatively characterize nuclear protein aggregation / fibrillation. (C, D) show mean values and standard deviations of three independent experiments. (E) Correlation of lamin B1 depletion with nuclear speckle and Congo red pattern characteristics is calculated by linear fit analysis. Expression values of

lamin B1 were determined by immunoblot analysis (shown in Supplemental Fig. S8). Mean values of three independent experiments (presented in C, D and Supplemental Fig. S8) were used to calculate correlations. The detailed correlation analysis is shown in Supplemental Fig. S9. A.u., arbitrary units; I-Hg, inorganic mercury; LB1, lamin B1.

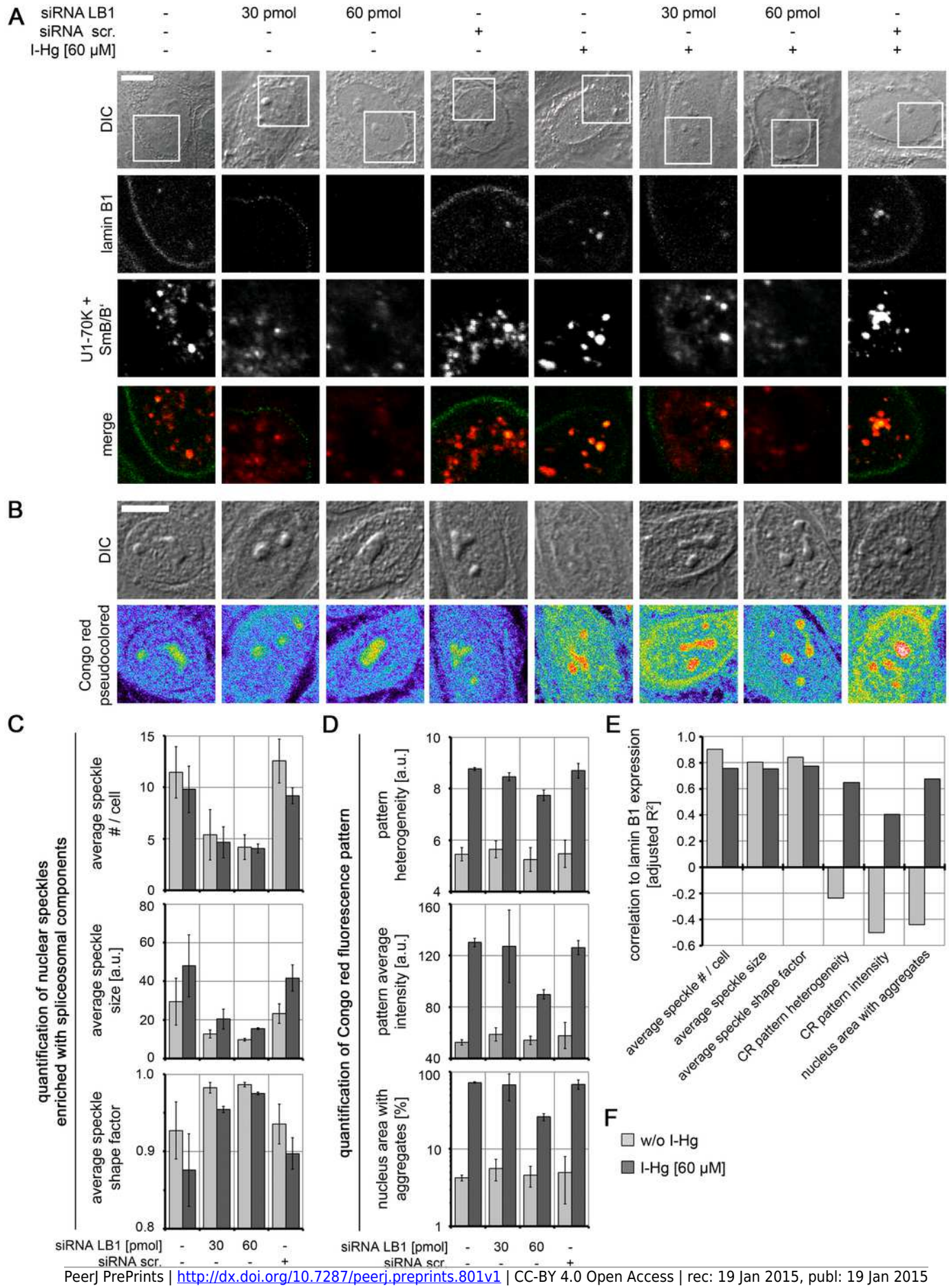

Table 1(on next page)

Hg concentrations as determined by atomic absorption spectroscopy (AAS).

Table 1. Hg concentrations as determined by atomic absorption spectroscopy (AAS). Total or I-Hg was determined in samples of *in vitro* exposed cells, laboratory animals or humans and wild animals that feed on marine diets.Total or I-Hg was determined in samples of *in vitro* exposed cells (HEp-2), laboratory animals or humans and wild animals that fed on marine diets. (*), 6*106 cells/ fraction, triplicated experiments; (**), T-Hg or I-Hg concentrations in different brain sites (cerebellum, occipital pole, pons, motor strip, frontal pole, thalamus and pituitary) were averaged for this table; obese and control monkeys were excluded; (***), I-Hg; (****), interquartile range. Bw, body weight; dw, dry weight; I-Hg, inorganic mercury; Me-Hg, organic mercury; T-Hg, total mercury; ww, wet weight.

Table 1. **Hg concentrations as determined by atomic absorption spectroscopy (AAS)**. Total or I-Hg was determined in samples of *in vitro* exposed cells, laboratory animals or humans and wild animals that feed on marine diets.

	Sample	n	T-Hg [µg/g ww]	T-Hg [µg/g dw]	Reference
HEp-2, w/o I-Hg	cytoplasm	*		0.07 ± 0.05	Here
HEp-2, w/o I-Hg	nucleus	*	0.06 ± 0.01	0.14 ± 0.03	Here
HEp-2, I-Hg [60 µM, 4h]	cytoplasm	*		0.94 ± 0.98	Here
HEp-2, I-Hg [60 µM, 4h]	nucleus	*	2.74 ± 1.03	6.08 ± 2.29	Here
Monkey *(Macaca fascicularis)*, Me-Hg [50 µg / kg bw, 6 months]	brain **	4	3.01 ± 0.28 (0.30 ± 0.15)***		Vahter et al, 1995
Monkey *(Macaca fascicularis)*, Me-Hg [50 µg / kg bw, 12 months]	brain **	4	4.32 ± 1.28 (0.43 ± 0.21)***		Vahter et al, 1995
Monkey *(Macaca fascicularis)*, Me-Hg [50 µg / kg bw, 18 months]	brain **	4	4.66 ± 0.57 (1.14 ± 0.61)***		Vahter et al, 1995
Human, mother, at parturition, Faroe Islands	hair	914		4.27 (2.6 - 7.7)****	Grandjean et al, 1997
Human, child, 12 month old, Faroe Islands	hair	527		1.12 (0.69 – 1.88)****	Grandjean et al, 1997
Human, child, 7 years old, Faroe Islands	hair	903		2.99 (1.7 – 6.1)****	Grandjean et al, 1997
Arctic foxes (*Vulpes lagopus*), juveniles, Iceland coastal	hair	6		4.02 ± 1.82	Bocharova et al, 2013
Arctic foxes (*Vulpes lagopus*), juveniles, Iceland inland	hair	5		4.50 ± 1.92	Bocharova et al, 2013
Arctic foxes (*Vulpes lagopus*), adult, Iceland coastal	hair	10		14.52 ± 2.51	Bocharova et al, 2013
Arctic foxes (*Vulpes lagopus*), adult, Iceland inland	hair	6		2.89 ± 1.31	Bocharova et al, 2013
Northern Fulmar (*Fulmarus glacialis*), Norway	liver	15	3.0 ± 2.7		Knudsen et al, 2007
Northern Fulmar (*Fulmarus glacialis*), North Pacific	liver	15		14.2 ± 10	Kim et al, 1996
Northern Fulmar (*Fulmarus glacialis*), North Pacific	kidney	5		6.7 ± 3	Kim et al, 1996
Northern Fulmar (*Fulmarus glacialis*), North Pacific	muscle	5		1.4 ± 1	Kim et al, 1996
Northern Fulmar (*Fulmarus glacialis*), North Pacific	feathers	17		4.8 ± 2.4	Kim et al, 1996
Northern fur seal (*Callorhinus ursinus*), Sanricu, Japan	liver	24		165 ± 132	Ikemoto et al, 2004
Northern fur seal (*Callorhinus ursinus*), Sanricu, Japan	kidney	20		4.4 ± 1.4	Ikemoto et al, 2004
Northern fur seal (*Callorhinus ursinus*), Sanricu, Japan	muscle	20		1.7 ± 0.5	Ikemoto et al, 2004
Northern fur seal (*Callorhinus ursinus*), Sanricu, Japan	hair	20		4.9 ± 1.1	Ikemoto et al, 2004

Table 2(on next page)

RNA processing factors that are components of the I-Hg-induced aggregome according to their occurence in different RNA maturation / splicing steps.

Table 2. RNA processing factors that are components of the I-Hg-induced aggregome according to their occurence in different RNA maturation / splicing steps.Aggregate components were listed by means of a spliceosome database (Cvitkovic and Jurica, 2013) according to their role in spliceosomal complexes. Positive identifications are marked by a black dot. *, HEp-2 ground state aggregome.

Table 2. RNA processing factors that are components of the I-Hg-induced aggregome according to their occurence in different RNA maturation / splicing steps.

	spliceosome/aggregate component	molecular weight (kD)	class/family	hnRNP	hnRNP/U2snRNP	SR protein	splicing factor	alternative splicing factor	EJC/mRNP	A complex	C complex	mRNA binding	RNA helicase	heat shock	nucleolus	transcription	translation	spliceosomal complexes: E	E'	A	A'	B	C	H	EDC-A	EDC-E	Bact	mixed	supra	U2	mRNP
*	n/a																														
HEp-2, I-Hg-induced aggregome	FUS	53.4	hnRNP	•														•	•	•	•	•	•	•	•	•		•	•		
	HNRPDL	46.4	hnRNP	•														•	•					•	•			•			
	HNRNPH1	49.2	hnRNP	•														•			•	•	•	•	•			•	•		
	HNRNPH3	36.9	hnRNP	•																		•			•			•	•		
	HNRNPC	33.7	hnRNP	•														•	•	•	•	•	•	•	•	•	•	•	•		
	RBMX	42.3	hnRNP	•														•	•	•		•	•	•	•		•	•	•		
	HNRNPK	51.0	hnRNP	•														•	•	•	•	•	•	•	•	•		•	•		
	HNRNPL	64.1	hnRNP	•														•	•		•	•	•	•	•			•	•		
	SYNCRIP	69.6	hnRNP	•														•	•	•	•	•	•	•	•	•		•	•		
	HNRNPR	70.9	hnRNP	•														•	•	•	•	•	•	•	•			•	•		
	HNRNPA1	38.7	hnRNP	•															•	•	•	•	•		•	•		•	•		
	HNRNPA2B1	37.4	hnRNP	•															•	•	•	•	•	•	•	•		•	•		
	SRSF1	27.2	SR protein			•												•	•	•		•	•		•			•	•	•	
	SRSF2	25.5	SR protein			•												•	•	•	•	•	•	•	•			•			
	SRSF10	31.3	SR protein			•																•	•				•	•	•		
	SFPQ	76.1	splicing factor				•												•			•	•	•	•			•			
	ALYREF	26.9	EJC/mRNP						•									•				•	•	•			•	•	•		•
	MATR3	94.6	C complex								•								•		•	•	•	•				•	•		
	DDX21	87.3	RNA helicase										•									•	•				•	•			
	DDX3X	73.2	RNA helicase										•									•	•	•			•	•	•		
	DDX5	69.1	RNA helicase										•					•	•	•	•	•	•	•		•	•	•			
	HSPA8	70.9	heat shock											•							•	•	•	•	•	•	•	•			
	NPM1	32.6	nucleolus												•													•	•		
SH-SY5Y, ground state aggregome	HNRNPDL	46.4	hnRNP	•														•	•					•	•			•			
	HNRNPC	33.7	hnRNP	•														•	•	•	•	•	•	•	•	•	•	•			
	HNRNPD	38.4	hnRNP	•														•	•	•	•	•	•		•	•		•	•		
	HNRPG	42.3	hnRNP	•															•	•		•	•	•	•			•	•		
	HNRNPK	51.0	hnRNP	•														•	•	•	•	•	•	•	•	•		•	•		
	HNRNPM	77.5	hnRNP	•														•	•			•	•	•	•			•	•		
	PCBP1	37.5	hnRNP	•														•	•	•		•	•	•	•			•	•		
	HNRNPR	70.9	hnRNP, U2snRNP		•													•	•	•	•	•	•	•	•	•	•	•	•		
	HNRNPU	90.6	hnRNP, U2snRNP		•													•	•	•	•	•		•	•	•		•	•		
	HNRNPA1	38.7	hnRNP, U2snRNP		•														•	•	•	•	•	•	•	•	•	•	•		
	HNRNPA2B1	37.4	hnRNP, U2snRNP		•													•	•	•	•	•	•	•	•	•		•	•		
	SRSF1	27.7	SR protein			•												•	•	•		•	•		•		•	•	•	•	
	SRSF3	19.3	SR protein			•													•	•		•	•		•	•	•	•	•		•
	SRSF7	27.4	SR protein, mRNP			•												•			•	•	•				•	•			
	SFPQ	76.1	splicing factor				•												•			•	•	•	•			•			
	DDX5	69.1	RNA helicase										•					•		•	•	•	•	•		•	•	•			•
	HSP90AA1	84.7	heat shock											•											•			•	•		
SH-SY5Y, I-Hg-induced aggregome	FUS	53.4	hnRNP	•														•	•	•	•	•	•	•	•	•		•	•		
	HNRNPH1	49.2	hnRNP	•														•			•	•	•	•	•			•	•		
	HNRNPH3	36.9	hnRNP	•																		•			•			•	•		
	RBMX	42.3	hnRNP	•														•	•	•		•	•	•	•		•	•	•		
	HNRNPL	64.1	hnRNP	•														•	•		•	•	•	•	•			•	•		
	SYNCRIP	69.6	hnRNP	•														•	•	•	•	•	•	•	•	•		•	•		
	PCBP1	37.5	hnRNP	•														•	•	•		•	•	•	•			•	•		
	RALY	32.5	hnRNP	•															•		•	•	•	•	•			•			
	NONO	54.2	splicing factor				•																•					•	•		
	ELAVL1	36.1	alt. splicing factor					•											•	•		•	•	•	•		•	•	•		
	FUBP1	67.6	alt. splicing factor					•													•							•			
	KHSRP	73.1	alt. splicing factor					•										•						•				•			
	PTBP1	57.2	alt. splicing factor					•										•	•		•		•	•				•	•		
	ALYREF	26.9	EJC/mRNP						•									•					•	•			•	•			•
	U2AF2	53.5	A complex							•								•	•	•	•	•		•	•	•	•	•	•		
	MATR3	94.6	C complex								•								•		•	•	•	•				•	•		
	RBM39	59.4	mRNA binding									•						•	•	•	•	•	•	•	•	•	•	•	•		
	DDX3X	73.2	RNA helicase										•									•	•	•			•	•	•		
	DHX9	141.0	RNA helicase										•					•			•		•					•	•		•
	HSPA8	70.9	heat shock											•							•	•	•	•	•	•	•	•			
	NPM1	32.6	nucleolus												•													•	•		
	RUVBL1	50.2	transcription													•							•				•		•		
	EEF1A1	50.1	translation														•		•				•		•	•	•	•			